THESIS FOR THE DEGREE OF DOCTOR OF PHILOSOPHY

Using Low Energy Light to Enable High Energy Photochemistry

WERA LARSSON

Department of Chemistry and Chemical Engineering
Chalmers University of Technology
Gothenburg, Sweden 2024

Using Low Energy Light to Enable High Energy Photochemistry
WERA LARSSON
ISBN: 978-91-8103-034-1

Doktorsavhandlingar vid Chalmers Tekniska Högskola
Ny serie nr: 5492
ISSN: 0346-718X

Department of Chemistry and Chemical Engineering
Chalmers University of Technology
SE-412 96 Gothenburg
Sweden
Telephone +46 31 772 1000

Cover: Illustration of light with different colors, reaching an energy barrier depicted as a wall. Only violet light has enough energy to inherently overcome this barrier, while other colors are transferred through the wall through light-manipulation. This manipulation is depicted through molecular structures and figures from the respective research projects that this thesis is based on.

Printed by Chalmers digitaltryck
Gothenburg, Sweden 2024

Using Low Energy Light to Enable High Energy Photochemistry

Wera Larsson
Department of Chemistry and Chemical Engineering
Chalmers University of Technology

ABSTRACT

Manipulating light to meet human needs is pivotal in various research fields and technological applications, ranging from solar energy conversion to photodynamic therapy and fluorescence imaging of cells and tissues. This thesis addresses the spectral mismatches between available light and the specific energy requirements of target photochemical reactions by employing low-energy light to control high-energy photochemistry. Central to this endeavor are molecular photoswitches, represented by diarylethene and spiropyran derivatives, which serve as model compounds across all discussed papers.

The experimental research presented herein explores three distinct methodologies: rapid fluorescence modulation, triplet sensitization, and triplet-triplet annihilation photon upconversion. Notably, the rapid modulation of fluorescence using a water-soluble diarylethene derivative enables the differentiation of fluorescence from a bright background, opening up for contrast-enhanced fluorescence imaging in cellular environments. Additionally, the realization of all-visible-light switching of diarylethenes through nanocrystal/molecular hybrid triplet sensitizers enhances the fatigue resistance of the diarylethene molecules.

Furthermore, the investigation into triplet-triplet annihilation photon upconversion reveals promising avenues for single-wavelength control of diarylethenes and water-compatible photochemistry, demonstrated by the isomerization and deprotonation of a spiropyran photoacid. While triplet sensitization relies on close molecular contact between light-manipulating species and photoreactants, photon upconversion allows for physical separation due to photons serving as energy carriers.

Building upon these advancements, further optimization and mechanistic understanding are necessary for these methods to realize their full potential. Nevertheless, the findings presented in this thesis bring us closer to achieving visible-light control of high-energy photochemical transformations, offering significant implications for both fundamental research and practical applications.

Keywords: solar energy conversion, photochemistry, molecular photoswitches, fluorescence modulation, triplet sensitization, photochemical upconversion, triplet-triplet annihilation

LIST OF APPENDED PAPERS

This thesis is based on the work contained in the following papers, referred to by Roman numerals in the text, ‡ indicate shared first authorship.

Paper I **Rapid amplitude-modulation of a diarylethene photoswitch: en route to contrast-enhanced fluorescence imaging**. Gaowa Naren,‡ Wera Larsson,‡ Carlos Benitez-Martin, Shiming Li, Ezequiel Pérez-Inestrosa, Bo Albinsson and Joakim Andréasson. *Chemical Science* **2021**, *12*, 7073-7078.

Paper II **A general approach for all-visible-light switching of diarylethenes through triplet sensitization using semiconducting nanocrystals**. Lili Hou, Wera Larsson, Stefan Hecht, Joakim Andréasson and Bo Albinsson. *Journal of Materials Chemistry C* **2022**, *10*, 15833-15842.

Paper III **Diarylethene isomerization by using triplet-triplet annihilation photon upconversion**. Wera Larsson, Masakazu Morimoto, Masahiro Irie, Joakim Andréasson and Bo Albinsson. *Chemistry - A European Journal* **2023**, *29*, e202203651.

Paper IV **Triplet-triplet annihilation photon upconversion in microcapsules: driving photochemistry using upconverted photons in water**. Wera Larsson, Viktor Eriksson, Fredrik Edhborg, Wilma Björkman, Jessica Johnsson, Jean Rouillon, Markus Andersson Trojer, Joakim Andréasson, Lars Evenäs and Bo Albinsson. *Manuscript*

CONTRIBUTION REPORT

Paper I Performed the photophysical measurements and data analysis with G.N. Wrote most of the manuscript. All synthesis related work was done by S.L. and microscopy measurements were done by C.B.M.

Paper II Performed some of the photophysical measurements together with L.H. and did part of the data analysis. Contributed to the manuscript. All synthesis related work was done by L.H. and S.H.

Paper III Conceptualized the project together with B.A. and J.A. Performed all the photophysical measurements and all data analysis. Planned the experiments together with J.A. and B.A. Wrote the manuscript. All synthesis related work was done by M.M. and M.I.

Paper IV Developed the project idea based on the conceptualization of F.E. and B.A. Performed most of the photophysical measurements and data analysis. Formulated and imaged some of the microcapsules, but main responsible for formulation and microscopy were V.E. and W.B. Wrote the manuscript. All synthesis related work was done by J.R.

LIST OF ABBREVIATIONS

3-PCA	Phenanthrene-3-carboxylic acid
CCD	Charge-coupled device
CdS	Cadmium sulfide
CW	Continuous wave
DAE	Diarylethene
DAEc	Closed form diarylethene isomer
DAEo	Open form diarylethene isomer
DET	Dexter energy transfer
DPA	9,10-diphenylanthracene
E_{photon}	Photon energy
eV	Electron volt
FRET	Förster resonance energy transfer
I_{th}	Excitation threshold intensity
IC	Internal conversion
IR	Infrared
ISC	Intersystem crossing
k_i	Rate constant of a process i
MC	Merocyanine
MCH	Protonated Merocyanine
NC	Nanocrystal
ns-TA	Nanosecond transient absorption
OLID	Optical lock-in detection
Φ_i	Quantum yield of a process i
PLGA	Poly(D,L-lactide-co-glycolide)
PMT	Photomultiplier tube
PSS	Photostationary state
PtOEP	Platinum octaethylporphyrin
S	Total spin
S_0	Singlet ground state
S_1	First singlet excited state
SP	Spiropyran
τ_i	Lifetime of a process i
T_1	First triplet excited state
TA	Transient absorption
TCSPC	Time-correlated single photon counting
TET	Triplet energy transfer

TIPS-An	9,10-bis[(triisopropylsilyl)ethynyl]anthracene
TTA	Triplet-triplet annihilation
TTA-UC	Triplet-triplet annihilation photon upconversion
UC	Upconversion
UCQY	Upconversion quantum yield
UV	Ultraviolet
Vis	Visible
VR	Vibrational relaxation
ZnOEP	Zinc octaethylporphyrin

CONTENTS

1

Introduction

Without light, we humans could neither perceive the world around us nor have a habitable planet to live on, nor food to eat, since plants and plankton would lack the electromagnetic energy to convert carbon dioxide and water to oxygen and chemical energy through photosynthesis.[1] Although the photochemical reactions that enable vision in our retina and photosynthesis in plants can be readily enabled by the light that is available from the sun and artificial lighting, this is not always the case for other photochemical processes. One can say that there is a spectral mismatch between the available light, and the light needed to efficiently control different photochemical processes, particularly man-made "artificial" ones.

A well-known example of the spectral mismatch between the available light and human needs is the utilization of sunlight in solar energy applications. Although sunlight is highly abundant on Earth,[2] only parts of the solar spectrum can be utilized in today's photovoltaic devices and solar fuel production. This is because conventional solar cells are made of semiconductors, with silicon being the most frequently used material today.[3] Silicon has a bandgap of 1.1 eV (approximately 1100 nm),[4] meaning that photons with lower energy than this will not lead to electricity production in the device and that photons with excess energy will give rise to thermalization losses. These losses limits the theoretical efficiency of single-junction silicon solar cells to just above 30%, known as the Shockley-Quisser limit.[5] Another example of how the sunlight reaching Earth does not perfectly match human needs is the production of solar fuels. Many of today's best performing systems for photoinduced catalytic water splitting typically relies on ultraviolet (UV) light catalysts, such as titanium dioxide to facilitate the hydrogen production.[6,7] Since a vast majority of the UV light coming from the sun is absorbed by the ozone layer, there is not a lot of photons reaching Earth that can efficiently enable the high energy photochemistry needed in solar fuel production.

Spectral mismatches between the light at hand and the desired application finds

relevance in more fields than solar energy, a large one being life science. Sometimes although the light has enough energy to facilitate the reaction it might never reach the target due to poor tissue penetration of high energy light.[8,9] An example of when this issue arises is in photodynamic therapy, in which light and photo-active compounds are combined to kill cancerous cells.[10] The high energy light needed to enable a photonic stimulus could also trigger other unwanted phenomena such as autofluorescence,[11] which can be troublesome when imaging cells and tissue using fluorescence microscopy since it lowers the signal-to-background ratio. Using a high energy light source can also cause photodegradation and phototoxicity, disadvantages that are relevant also in non-biological applications.

Instead of being limited by the light at hand and adjusting the probes and materials, manipulating and modulating light to match the energetic requirements can be a way forward. There are several ways of altering light to overcome the spectral barriers exemplified above. While some research focuses on down-converting photons through the process of singlet fission to e.g. reduce the above mentioned thermalization losses in photovoltaics,[12] the focus of this thesis will be to utilize lower energy light to enable higher energy photochemistry. The higher energy photochemistry exemplified in this thesis is centered around controlling the photoisomerization and fluorescence of photochromic molecules, also referred to as molecular photoswitches.[13,14] In this work, these molecules serve both as model compounds, to demonstrate how to enable high energy photochemistry with low energy light, and as a suggested tool for further applications.

In addition to utilizing the molecular kinetic and spectral features of a photoswitch, one can also use other methods to enable high energy processes with lower energy light. A well-known example of this is triplet sensitization, in which a triplet sensitizer is excited by low energy light and transfers its excited state energy to the photoreactant through triplet energy transfer (TET).[15,16] In this thesis, I show how a photoisomerization reaction of a photoswitch requiring UV light can instead be enabled using visible light by utilizing the lower energy triplet manifold.[17] Since triplet sensitization involves the use of molecules as energy carriers, this way of enabling higher energy reactions requires the photoreactant and the sensitizers to be in physical contact. To allow for physical separation, one can use photon upconversion techniques so that the energy will instead be carried by photons. There are several ways of upconverting lower energy photons into higher energy photons, including two-photon absorption,[18] second harmonic generation,[19] and lanthanide-based upconverting nanoparticles.[20] These methods have proven useful in the field of photon upconversion, but a drawback with them is that they are limited to coherent and high intensity lasing light sources. In this

thesis, photon upconversion has instead been done through the process of triplet-triplet annihilation photon upconversion (TTA-UC).[21–23] Since TTA-UC can occur using low-intensity non-coherent light, this photon upconversion method also opens up for solar energy applications.[24–26]

1.1 Outline and Scope of Thesis

This thesis contains different approaches to using low energy light to enable high energy photochemical reactions and photophysical processes. The theoretical framework of the research in this thesis is presented in Chapter 2, spanning from the fundamentals of light-matter interactions to the materials and photochemical processes used in the papers on which this thesis is based. The findings in this thesis are based on experimental research, and Chapter 3 contains a summary of the experimental methods used. Chapter 4 is based on **Paper I**, in which the fluorescence of a water soluble diarylethene (DAE) photoswitch is rapidly modulated by light absorbed by the non-fluorescent isomer, rather than the fluorescent isomer. As a result, lock-in amplification can be used to separate the modulated DAE fluorescence from a bright background, opening up for novel applications in fluorescence microscopy. In **Paper II**, triplet sensitization, using hybrids of nanocrystals (NCs) and organic mediators, is used to enable all-visible-light control of DAEs, resulting in less photodegradation as compared to using UV light. The findings of this paper are presented in Chapter 5. Instead of using molecules or particles as energy carries, such as in triplet sensitization, **Paper III** and **Paper IV** show how photons can carry the photochemistry enabling energy through TTA-UC, which is presented in Chapter 6. **Paper III** also focuses on the isomerization of DAEs. By using TTA-UC, a single light source can be used to trigger both reversible photoisomerization and fluorescence of the DAEs. The final work presented in this thesis is **Paper IV**, in which the TTA-UC is performed in core-shell microcapsules dispersed in water as a means to utilize the upconverted photons to facilitate photochemical reactions in a more efficient way. The upconverting microcapsules were used to enable the isomerization and deprotonation of a spiropyran/merocyanine (SP/MC) photoacid. Conclusions of the findings presented in Chapters 4-6 and an outlook on future research within the scope of this thesis is presented in Chapter 7.

2

Fundamentals

A fundamental concept for the research presented in this thesis is light-matter interactions. In this Chapter, the theory behind these interactions will be presented, together with the photochemical processes and materials central for the thesis.

2.1 Light-Matter Interactions

Light can be described as an oscillating electromagnetic wave. This electromagnetic field is a combination of an oscillating electric and an oscillating magnetic field that propagates in the same direction, as illustrated in Figure 2.1. The distance between two consecutive maxima is defined as the wavelength, λ, of light. Since the oscillating electric field can interact with electrons in atoms and molecules, it is this wave component that is of primary interest in optical spectroscopy.[27]

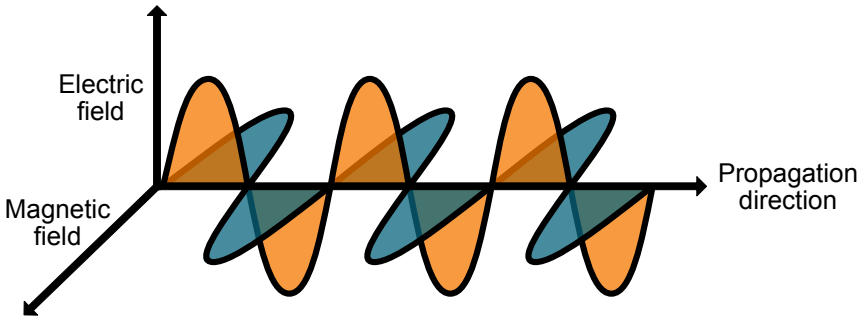

Figure 2.1: Illustration depicting the propagation of an electromagnetic wave as a combination of an electric and a magnetic field perpendicular to each other, propagating in the same direction.

A light particle is called a photon, and the two ways of describing light as both an electromagnetic wave and a photon constitutes the wave-particle duality. The energy, E_{photon}, carried by a photon is discrete and is related to the wavelength,

λ, or the frequency, ν, of the electromagnetic field through the Planck constant, h, and the speed of light, c. This relation is shown in Equation (2.1).[27,28]

$$E_{photon} = \frac{hc}{\lambda} = h\nu \tag{2.1}$$

Looking at this equation, it is evident that light with shorter wavelengths has higher energy than light with longer wavelengths. The electromagnetic spectrum is divided into different wavelength regions, with three of them being relevant for the methods used in this thesis: the ultraviolet (UV), visible, and infrared (IR). Light that can be perceived by the human eye is referred to as visible light, and covers wavelengths of approximately 400-750 nm. This spectral region is flanked by UV light (shorter wavelengths) and IR light (longer wavelengths).

2.1.1 Electronic States

Atoms consist of a nucleus built up of neutrons and positively charged protons, with negatively charged electrons surrounding the nucleus. These electrons can possess discrete quanta of energy, and are organized in atomic orbitals. When atoms are combined to form molecules, the atomic orbitals form molecular orbitals. Pauli's exclusion principle states that only one electron can occupy a specific quantum state in a system. As a consequence of this, a maximum of two electrons can be in the same orbital and only on the condition that they have opposite spin. If this is the case, it is said that the electrons are paired. With electrons being fermions, their spins can be either $\pm\frac{1}{2}$. The sign determines the direction of the spin, which commonly is referred to as spin up or spin down. The total spin, S, is the sum of the electron spins and can take on values of 0 or 1 in a two-electron system as given from the Clebsch-Gordan series. If the electrons are paired ($S = 0$), the molecule is said to be in a singlet state and if they are unpaired ($S = 1$) it is said to be in a triplet state. Figure 2.2 shows an illustration of the electron configuration in a two-electron system for a singlet ground state, a singlet excited state and a triplet excited state. The multiplicity of the electronic states is defined as $2S+1$, and this is where the words singlet and triplet originates from since they have the multiplicity of one and three, respectively.

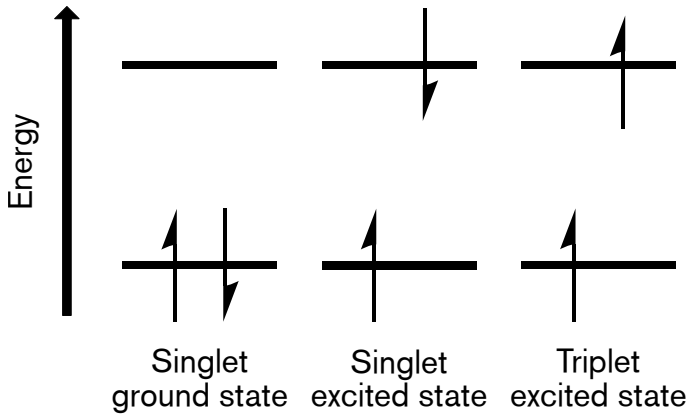

Figure 2.2: Diagram illustrating the electronic structure of singlet and triplet states, with electrons represented as half-arrows indicating their spin direction.

Most molecules have a singlet ground state, with the possibility of having both singlet and triplet excited states depending on the spin pairing. All of these types of electronic states will be of importance in the photophysical processes that are relevant for this thesis, as will be shown in the following sections. An important exception to having a singlet ground state is the oxygen molecule, which instead has a triplet ground state.[29] This is made possible by the fact that molecular orbitals can be degenerate, meaning that multiple orbitals can have the same energy. Hund's rule states that if there are multiple orbitals with the same energy, they will first be singly occupied with electrons with parallel spin before being doubly occupied. In a molecule with e.g. two degenerate orbitals and two available electrons, this will lead to a triplet ground state with two unpaired electrons distributed in each of the orbitals.

2.1.2 Radiative and Non-Radiative Transitions

After elucidating the properties of both light and matter in the preceding sections, the focus now shifts to the interaction between the two. As seen in Figure 2.2, the promotion of an electron to a higher energy orbital leaves the atom or molecule in a higher electronic excited state. This excitation event can be induced by e.g. the absorption of a photon. For this to occur, the energy of the absorbed photon must match the energy difference between the two states. This energy conservation criteria is called Bohr's frequency condition, and this must also be fulfilled when a photon is emitted from an electronically excited atom or molecule.[27]

Upon absorption of a photon, the molecule can undergo several different relaxation pathways to return back to its ground state. A Jablonski diagram showing some of these photophysical processes is displayed in Figure 2.3, for a molecule with

a singlet ground state (S_0). The absorption of a photon (blue arrow) occurs in less than a femtosecond, and typically leads to the molecule being excited to a higher vibrational level of its first singlet excited state (S_1). This absorption event is followed by vibrational relaxation (VR) (wavy grey arrow) to S_1. From S_1, the molecule can decay to S_0 through radiative and non-radiative pathways. The energy can be released as emitted light through fluorescence (green arrow), which occurs on a timescale of nanoseconds. Non-radiative relaxation can occur through internal conversion (IC) (dashed black arrow) to a high vibrational energy level of S_0, followed by VR to the lowest vibrational energy level. Another decay pathway from S_1 is through intersystem crossing (ISC) to the first triplet excited state (T_1), followed by phosphorescence (red arrow). ISC and phosphorescence are said to be spin-forbidden processes, since they involve a spin flip of an electron to go between singlet and triplet states. This means that the lifetime of phosphorescence (i.e. the time the molecule will reside in its excited state) will be longer than that of fluorescence with typical timescales of micro- to milliseconds. ISC to T_1 can also be followed by VR to S_0, making the molecule decay non-radiatively.

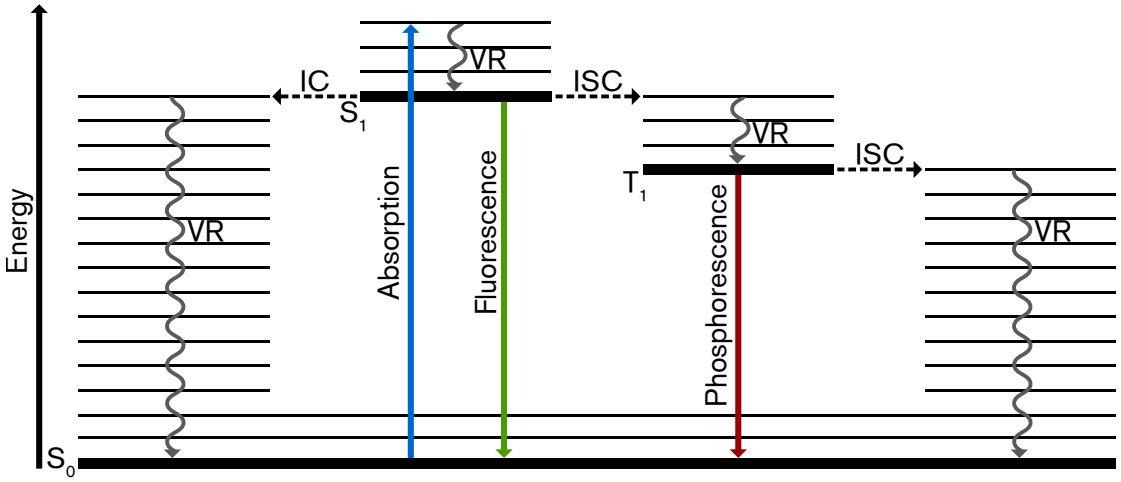

Figure 2.3: Jablonski diagram illustrating photophysical processes that can occur between the singlet ground state (S_0) and the first singlet (S_1) and triplet excited states (T_1). Thick black horizontal lines denote electronic states, while thin black lines represent vibrational energy levels. The depicted processes (arrows) include absorption, vibrational relaxation (VR), fluorescence, internal conversion (IC), intersystem crossing (ISC), and phosphorescence.

In optical spectroscopy, there is often a need to quantify the photophysical processes that take place in the studied systems. A central way of doing this is by determining the quantum yield (Φ_i) of the process i, which is defined as shown in Equation (2.2).

$$\Phi_i = \frac{number\ of\ events}{number\ of\ photons\ absorbed} = \frac{k_i}{\Sigma_j k_j} \tag{2.2}$$

k_i is the rate constant of the investigated process, and the quantum yield is found by dividing k_i with the sum of the rate constants of all possible deactivation pathways that can deactivate the state ($\Sigma_j k_j$). Another parameter of great interest within optical spectroscopy is the lifetime of a certain excited state (τ_i), i.e. the average time a molecule will stay in this state. It is defined as the inverse sum of all the rate constants of all possible deactivation pathways that can deactivate the state, as seen in Equation (2.3).

$$\tau_i = \frac{1}{\Sigma_j k_j} \tag{2.3}$$

2.2 Processes and Materials Central for This Work

Having outlined the background about light-matter interactions within single molecules, specific processes and materials most relevant for this thesis will be explained in the following sections.

2.2.1 Intermolecular Energy Transfer

The excited state energy of a molecule can, on top of being released through the decay pathways presented in Figure 2.3, be transferred to other molecules. Förster resonance energy transfer (FRET) is governed by Coulumbic dipole-dipole interactions between a donor and an acceptor molecule.[30] Dexter energy transfer (DET) on the other hand, can be seen as a virtual electron exchange between the donor and acceptor molecule.[31] DET requires a spatial orbital overlap between the involved molecules, and is hence limited to short distances between the donor and acceptor molecule (typically a few Å) while FRET can occur over slightly longer distances (typically a few nm). The energy transfer mechanism of primary interest in this thesis is DET, which is illustrated for a triplet energy transfer (TET) event in Figure 2.4. A triplet excited donor molecule (^{3}D*) transfers its energy to a ground state acceptor molecule (A), resulting in a ground state donor molecule (D) and a triplet excited acceptor molecule (^{3}A*). As seen in the figure, the spin multiplicity of both the donor and acceptor molecules change during this TET. But since the total spin angular momentum of the whole system is preserved, it will still be a spin-allowed process.

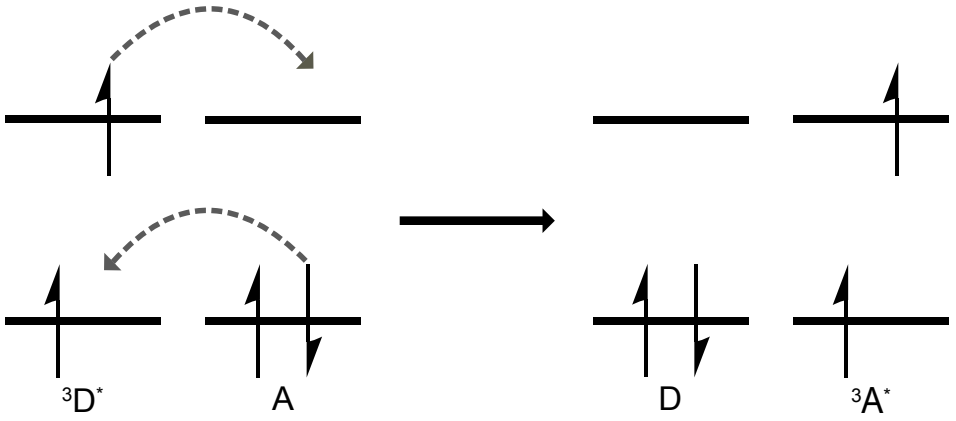

Figure 2.4: Dexter energy transfer depicted as a virtual electron exchange between a triplet excited donor molecule (^{3}D*) and a ground state acceptor (A), yielding a ground state donor molecule (D) and a triplet excited acceptor molecule (^{3}A*).

2.2.2 Molecular Photoswitches

As outlined in Chapter 1, the higher energy photochemistry exemplified in this thesis is the photoisomerization of photochromic molecules. These types of molecules, also referred to as molecular photoswitches, can be reversibly transformed between two isomers. Generally, this reversible isomerization is photoinduced (i.e. photoisomerization) in both directions, but for some molecules one of the isomerization directions can be thermally induced. Isomerization leads to structural changes in the photochromic molecule, leading to changes in absorption and fluorescence spectra together with other property changes such as redox energies and dipole moments.[14]

The molecular photoswitches used in **Papers I-III** all belong to one of the major families of photochromic molecules, namely diarylethenes (DAEs).[32–34] Figure 2.5 shows the structure and isomerization scheme of the DAEs in **Paper III**. UV light irradiation of the colorless open form isomer (DAEo) can facilitate a ring-closing reaction to the colored closed form isomer (DAEc). Since DAEc absorbs strongly also in the visible region, the reverse ring-opening reaction can be facilitated using a visible light source. During the isomerization reaction, a rearrangement of single and double bonds takes place in what is called a cyclization reaction. As previously mentioned, these structural changes will influence the emissive properties of the DAEs. All DAEs in this thesis have one strongly fluorescent isomer, either the open form (**Paper I**) or the closed form (**Papers II** and **III**). DAEs have found their way into various applications, including optical memories,[35] organic light-emitting transistors,[36] and bioimaging.[37] Their widespread use can be explained by properties like thermal stability towards degradation, high fatigue-resistance

over repeated isomerization cycles, efficient cyclization process, and rapid response together with reactivity in the solid state.[34,38]

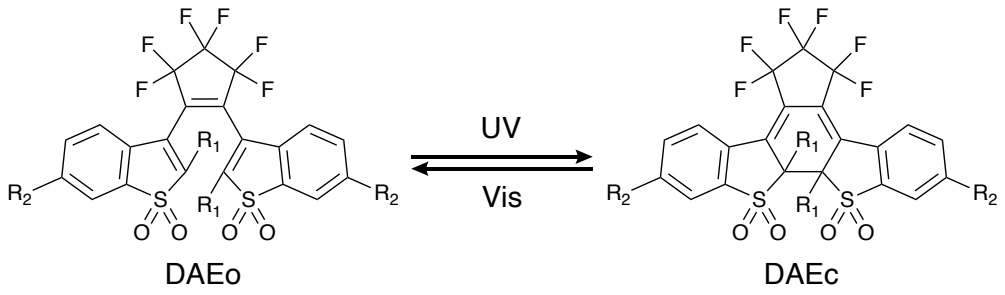

Figure 2.5: Structure and isomerization scheme of the DAEs in **Paper III**, illustrating the UV light-induced isomerization from the open isomer DAEo to the closed isomer DAEc, and the reverse isomerization induced by visible light.

In **Paper IV**, another type of molecular photoswitch is used. Here, the molecule belongs to the spiropyran (SP) family of photochromic molecules. They were discovered even earlier than DAEs, and have also been thoroughly studied and used over the years.[39] In contrast to the DAEs, it is the closed spiropyran isomer that is colorless, while it is the open form isomer (known as the merocyanine (MC) form) that is colored and absorbs strongly also in the visible region. For structures and isomerization scheme of the photoswitch used in this study, refer to Figure 6.7c. As with DAEs, the spiropyrans can undergo reversible photoisomerization but due to a typically lower energy barrier for the thermal back-reaction from MC to SP they are less thermally stable than DAEs.[14] The spiropyran photoswitch used in **Paper IV** can also be used as a photoacid, meaning that light can also induce a deprotonation reaction, leading to light- and thermally induced pH changes when the concentration of the molecules are kept high enough.[40,41] As with DAEs, spiropyrans have also found use in applications in diverse fields such as photoresponsive materials,[42] optical data storage,[43] and drug delivery systems.[44]

2.2.3 Triplet Sensitization

Sensitization constitutes the process by which a molecule, termed as a sensitizer, absorbs light energy and subsequently transfers this excited state energy to an adjacent molecule while returning to its ground state.[15,16] This thesis will focus on the process of triplet sensitization in which a triplet sensitizer is first excited to a singlet excited state, before it relaxes to a lower energy triplet excited state. The excited state energy is then transferred through TET to an acceptor molecule that will consequently become triplet excited. For this process to transpire efficiently, the sensitizer needs to have a high molar absorptivity, a rapid ISC, and a

small energy gap between the singlet and triplet excited states to minimize thermal losses. The TET event between the sensitizer and acceptor requires a close proximity between the molecules. This can be achieved by physically linking the sensitizer to the acceptor.[45–48] Another option is to have the two molecules in the same solution, making the sensitization diffusion-controlled.[49] This necessitates a sufficiently prolonged triplet lifetime of the sensitizer, typically ranging from microseconds to milliseconds, to allow for the sensitization process. As mentioned previously, oxygen has triplet ground states, making it particularly efficient in quenching triplet states, hence requiring oxygen-free samples to avoid quenching effects.[50–52]

2.2.4 TTA-UC

Photon upconversion is the conversion of lower energy light into light of higher energy. The photon upconversion method employed in this thesis is known as triplet-triplet annihilation photon upconversion (TTA-UC), a process wherein two lower energy photons undergo conversion into one higher energy photon through a sequence of energy transfer events.[21–23] Similar to the previously described triplet sensitization process, TTA-UC relies on triplet excited states, thereby making molecular oxygen a quencher for this process as well. Illustrated in Figure 2.6, a Jablonski diagram elucidates the underlying mechanism behind TTA-UC.

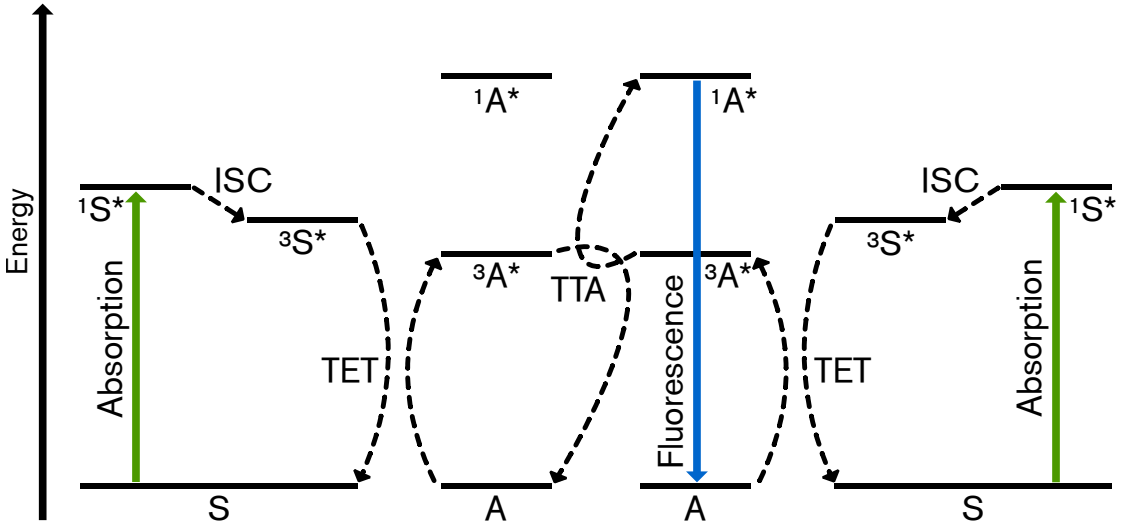

Figure 2.6: Jablonski diagram illustrating the TTA-UC process, from initial light absorption by a sensitizer molecule to the emission of higher-energy fluorescence from an annihilator molecule, encompassing intersystem crossing, triplet energy transfer, and triplet-triplet annihilation.

The TTA-UC process is initiated by the absorption of light (indicated by green ar-

rows) by a sensitizer molecule (S). This transitions the sensitizer to its first singlet excited state (^{1}S*), and is followed by ISC to its first triplet excited state (^{3}S*). It is imperative for a sensitizer to have a high ISC rate to efficiently generate triplet excited states. Subsequently, the triplet energy of the sensitizer is transferred to a ground state annihilator molecule (A) through TET. This leaves the annihilator in its first triplet excited state (^{3}A*). Two triplet excited annihilators can then undergo triplet-triplet annihilation (TTA), resulting in one annihilator returning to its ground state and the other being excited to its first singlet excited state (^{1}A*). In the final step of TTA-UC, a photon of higher energy than the two initially absorbed photons can be emitted as fluorescence (indicated by the blue arrow), while the annihilator relaxes to its ground state. Given that both the TET and TTA processes are diffusion-controlled in liquid solutions, it is essential for both the sensitizer and the annihilator to exhibit sufficiently long triplet lifetimes, typically on the order of microseconds to milliseconds, for these processes to unfold. The energy of the ^{1}A* state cannot be more than twice that of the ^{3}A* state for the TTA event to be energetically allowed.

To further illustrate the TTA-UC process, Figure 2.7 shows the time-resolved emission from a degassed upconversion sample containing the annihilator 9,10-diphenylanthracene (DPA) and the sensitizer platinum octaethylporphyrin (PtOEP) (the same TTA-UC pair that is used in **Paper III**). The sample was excited by a 532 nm pulsed laser, and the two figures show how the emission from the two upconversion chromophores evolve over time. Figure 2.7a shows the first 20 µs, during which the initial directly excited PtOEP phosphorescence decays and the upconverted DPA fluorescence rises to its maximum. The temporal evolution over 1 ms is shown in Figure 2.7b, during which the upconverted DPA emission decays until the excited states are completely depleted.

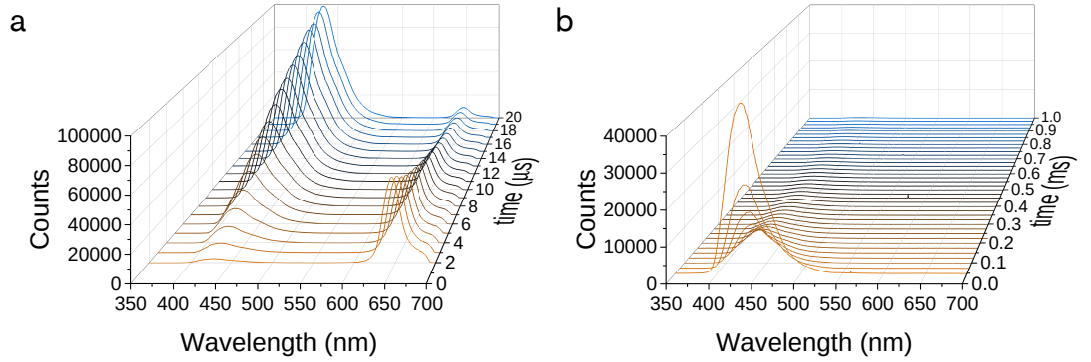

Figure 2.7: Time evolution of the TTA-UC process, illustrated as the time-resolved emission from a degassed upconversion sample containing 9,10-diphenylanthracene (DPA) ($\lambda_{em,max}$ = 426 nm) and platinum octaethylporphyrin (PtOEP) ($\lambda_{em,max}$ = 645 nm) as a result of 532 nm pulsed excitation. (a) The first 20 µs, during which the initial PtOEP emission decays and the upconverted DPA emission rises to its maximum. (b) The first 1 ms, during which the upconverted DPA emission decays.

With two lower energy photons being converted into one higher energy photon, the quantum yield of upconversion (UCQY) can theoretically not be higher than 50%.[53] As of today, the highest reported UCQY is 42% for red-to-green TTA-UC,[54] and the highest reported visible-to-UV UCQY is 17%.[55] TTA-UC performs well under low-intensity noncoherent light, such as sunlight, opening up for applications such as enhancing the efficiency of solar cells,[56–60] and producing solar fuels.[61–66] While this thesis does not delve into the mechanistic intricacies of TTA-UC or the development of new sensitizers or annihilators, it utilizes TTA-UC as a tool in **Paper III** and **IV** to control the photoisomerization of DAE and SP/MC photoswitches.

2.2.5 Microcapsules

When TTA-UC is performed in solution, the concentration of the chromophores needs to be high enough to enable the diffusion-controlled bimolecular energy transfer steps efficiently. One strategy to mitigate the re-absorption of upconverted photons that typically follows the use of high chromophore concentrations, is to encapsulate the TTA-UC system into smaller volumes dispersed in a solution.[67–74] This means that the high local concentrations of annihilator and sensitizer molecules can be maintained, whilst the total concentration and hence the re-absorption is kept low. This was was done in **Paper IV** by placing the upconversion chromophores in core-shell micrometer sized capsules, with a polymer shell made up of poly(D,L-lactide-co-glycolide) (PLGA) and an oil core made up of glyceryl trioctanoate. These capsules will be referred to as microcapsules in this

text, and Figure 2.8 shows a schematic illustration of them being dispersed in a solution (left) and an enlargement of the core-shell structure (right).

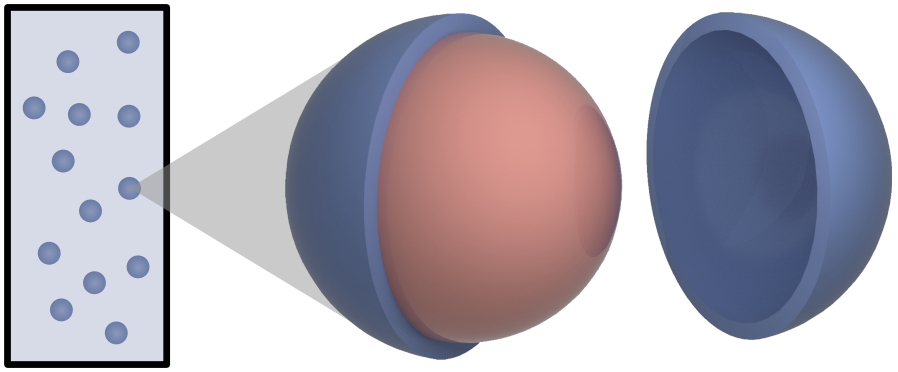

Figure 2.8: Illustration of microcapsules in solution (left) with an enlarged capsule showing the core-shell structure (right).

The developement of the microcapsule system and the formulation procedure will not be covered in this thesis, since they here merely function as tools for making efficient use of upconverted photons. It should still be noted that the method is fairly simple, and based on a well-established formulation procedure[75] with some modifications.[76] Briefly, the formulation is based on internal phase separation by solvent evaporation, and results in microcapsules with diameters around 10 µm with the annihilator and sensitizer molecules being primarily located in the oil core.

3

Experimental Techniques

Optical spectroscopic techniques have been the primary tools for the experimental work that has been conducted in this thesis. This Chapter provides a brief overview of different techniques together with examples of how the instrumentation was used in the different research projects.

3.1 UV-Vis Steady-State Absorption Spectroscopy

UV-Vis steady-state absorption spectroscopy stands as a pivotal method for analyzing the absorption properties of substances across specific wavelengths within the ultraviolet-visible (UV-Vis) spectrum. The absorbance at certain wavelengths is determined by measuring the intensity of light that passes through a sample. An illustration showing how a spectrophotometer works is depicted in Figure 3.1.

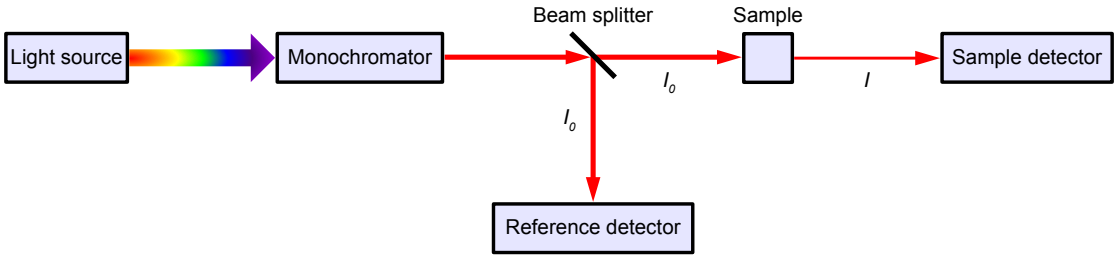

Figure 3.1: Illustration of a UV-Vis steady-state absorption setup.

In the spectrophotometer, a beam of light, known as the probe light, is passed through a monochromator, a device designed to isolate specific wavelengths of light, before reaching the sample. The intensities of light both before, I_0, and after, I, passing the sample are measured by a reference detector and a sample detector, respectively. The relationship between these intensities and the absorbance, A, is governed by the Lambert-Beer law, as represented in Equation (3.1). The Lambert-Beer law also elucidates how the absorbance of a sample is linearly dependent on the concentration of the absorbing species, c, the path length through

which light travels in the sample, l, and the molar absorptivity, ε, at the specific wavelength.[77]

$$A = log_{10}\left(\frac{I_0}{I}\right) = \varepsilon cl \tag{3.1}$$

An absorption spectrum can be generated by allowing the monochromator to scan across a spectrum of wavelengths, and serves as a valuable resource elucidating the composition of a sample, unveiling the presence of distinct species and quantifying their concentrations. UV-Vis steady-state absorption spectroscopy can also be used to monitor absorbance changes of reactive species over time, hence also making it a tool to determine slow reaction kinetics.

3.2 Transient Absorption Spectroscopy

To study the absorption of excited states, time-resolved absorption measurement techniques need to be used. In **Paper II**, nanosecond transient absorption (ns-TA) spectroscopy was used to monitor the decay of non-emissive triplet excited states. Figure 3.2 illustrates a typical ns-TA setup, in which the sample is excited using an intense pulsed laser (pump) whilst also being subjected to a weaker and often broadband pulse (probe). The detector records the transmitted probe light with and without the excitation from the pulsed pump laser, which gives the resulting differential absorption spectrum, ΔA. Equation (3.2) shows how ΔA is defined as the difference in absorbance with, A_+, and without, A_-, the pulsed laser excitation, and can be calculated using the intensity of the probe light that is transmitted through the sample with I_+ and without I_- the preceding pump pulse.

$$\Delta A = A_+ - A_- = log_{10}\left(\frac{I_-}{I_+}\right) \tag{3.2}$$

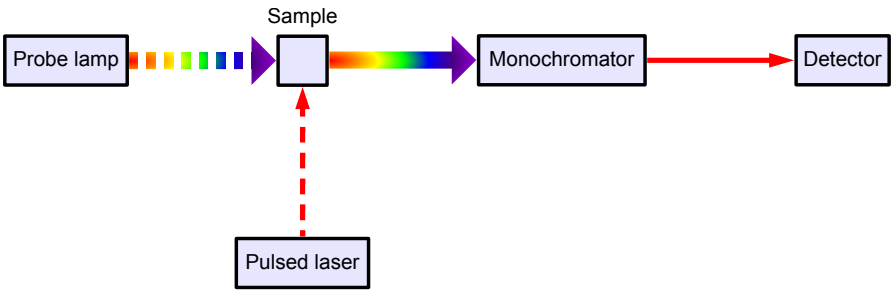

Figure 3.2: Illustration of a transient absorption setup. Note that the type of detector used varies with the type of measurement that is performed.

A photomultiplier tube (PMT) can be employed to record single-wavelength time-resolved decays, preceeded by a monochromator that isolates the desired wavelenght. Alternatively, to record an entire TA spectrum, a gated charged-coupled device (CCD) camera can serve as the detector. By adjusting the delay time, the temporal evolution of spectral features can be explored.

TA spectroscopy and emission spectroscopy, which will be explained shortly, can both be used to study quenching of excited states. This can be done either through measuring the lifetime of an emissive or non-emissive excited state, or through the steady-state emission intensity. In the case of a linear relationship between the lifetime (or emission intensity) and the concentration of the quencher, the rate constant of the energy transfer event can be elucidated using the Stern-Volmer equation as defined in Equation (3.3).[77]

$$\frac{\tau_0}{\tau} = \frac{I_0}{I} = 1 + \tau_0 k_q [Q] \tag{3.3}$$

τ_0 and τ represent the lifetimes in the absence and presence of the quencher, respectively. I_0 and I are their emission intensity counterparts. The bimolecular quenching rate constant (k_q) and the quencher concentration ([Q]) are also involved in this equation.

3.3 Steady-State Emission Spectroscopy

The determination of steady-state emission from a sample parallels the methodology employed in UV-Vis steady-state absorption spectroscopy. Illustrated in Figure 3.3, the setup involves subjecting the sample to monochromatic light, achieved either through a combination of white light with an excitation monochromator or via a continuous wave (CW) laser light source. Positioned after the sample is an emission monochromator, selecting the wavelength of light for detection. Emission is typically measured with the detector at a right angle relative to the excitation light, but since there typically is an overlap between the absorption and emission of the chromophores in an emissive sample, high concentrations can lead to inner-filter effects that influence the recorded emission signal.[77] The primary inner-filter effect constitutes the absorbance of the excitation light before reaching the detection point of the sample, leading to a decreased emission signal. When the emitted light is re-absorbed by the sample before reaching the detector the secondary inner-filter effect can change the shape of the emission spectrum. To mitigate these inner-filter effects, a front-face setup can be used in which the excitation light and the detector are facing the same (front) side of the sample.

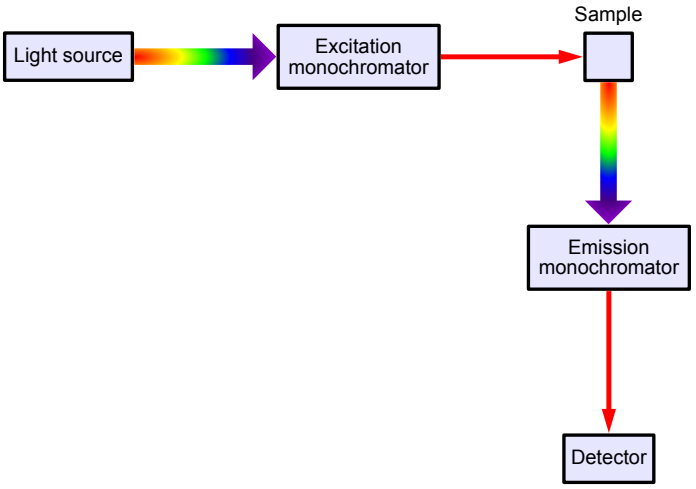

Figure 3.3: Illustration of a steady-state emission setup.

With a monochromator on either side of the sample, two types of spectra can be measured using steady-state emission spectroscopy. One type of measurement is done by keeping the emission monochromator fixed at a single wavelength and allowing the excitation monochromator to scan over a range of wavelengths. This provides an excitation spectrum, which typically mimics the absorption spectrum of the sample. Conversely, sweeping the emission monochromator while maintaining the excitation light at a fixed wavelength absorbed by the sample yields an emission spectrum. Variations in lamp intensity and detector sensitivity over the recorded wavelength region need to be accounted for using reference detectors and correction files.

Steady-state emission spectroscopy serves diverse purposes, including the determination of fluorescence quantum yields and the investigation of emission quenching phenomena. By monitoring the emission intensity over time, it can also be used to study reaction kinetics. Notably, fluorescence spectroscopy exhibits a very high level of sensitivity, surpassing absorption spectroscopy in detecting even minute concentrations of emissive species. In **Paper I** this sensitivity is detrimental when the combination of lock-in amplification and steady-state emission spectroscopy is used to discern a fluorescence-modulated signal amid a highly fluorescent background.

3.4 Time-Resolved Emission Spectroscopy

Time-resolved emission spectroscopy can be used to measure the lifetime of emissive species, by recording how the emission intensity decays over time. The time scale of the decay determines what technique needs to be used and depending on

the complexity of the excitation process, different fitting equations needs to be used to determine the lifetime of interest. Prompt fluorescence from direct excitation typically decays on a nanosecond timescale, and in a homogeneous sample with only one emissive species the decay is monoexponential. This means that the recorded emission decay can be fitted using Equation (3.4), where t is the time and τ is the lifetime. Additional exponential terms need to be added to the fitting equation if the sample contains multiple species that emits at the recorded wavelength or if, e.g., heterogeneity in the sample makes molecules decay at different rates.

$$I(t) = Aexp\Big(-\frac{t}{\tau}\Big) \tag{3.4}$$

Two different experimental techniques were used to measure emission lifetimes in this thesis, both initiated by excitation of the sample with a short excitation pulse. The fast fluorescence decays described above were recorded using time-correlated single photon counting (TCSPC), in which a pulsed laser diode is used to excite the sample. This is followed by the emission of photons from the sample, and the time delay between the laser pulse and when the first of the emitted photons reaches the detector is recorded. This is repeated for very many laser pulses, with the recorded decay times eventually making up a histogram with each data point representing the first emitted photon reaching the detector in each cycle.

Phosphorescence and TTA-UC with lifetimes on the micro- to millisecond timescale would be very time consuming to measure using TCSPC, since the measurement cycles needed to record every single photon would lead to very long measurement times. These types of samples were instead excited by a modulated CW laser, and square-shaped pulses were generated by coupling the laser diode to a pulse-generator. A PMT was then used to record the emission decay, during the time that the laser was turned off. Figure 3.4 illustrates both the TCSPC and the modulated CW laser measurements setup, with differences between the two being the excitation source and the detector.

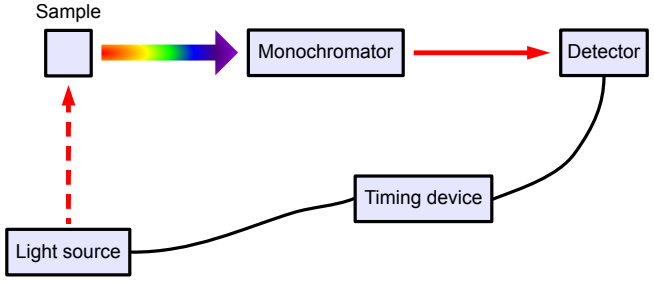

Figure 3.4: Illustration of a time-resolved emission setup.

When fitting TTA-UC decays, additional parameters need to be taken into account in the fitting equation as compared to a simple exponential decay. As seen in Equation (3.5), the emission intensity, $I(t)$, is proportional to the square of the triplet excited annihilator concentration at time t, $[^3A^*(t)]$. This is in turn dependent on the annihilator triplet concentration at time zero, $[^3A^*]_0$, the inherent triplet lifetime of the annihilator, τ_T, and the dimensionless parameter, β that indicates what fraction of triplets that initially decay by second-order channels (annihilation) ($0 < \beta < 1$). By recording the upconversion emission decay over a range of excitation intensities, a global fit of all decays with a shared τ_T can provide β for the different decay traces.[78] By determining the excitation intensity that corresponds to $\beta = 0.5$ (i.e. when equal amounts of annihilators decay by first- and second-order decay channels), one can find the threshold excitation intensity, I_{th}, for the TTA-UC system. A low I_{th} value is often desired, since it is defined as the excitation intensity needed to achieve 50% of the system-specific UCQY.[78,79]

$$I(t) \propto [^3A^*(t)]^2 = \left([^3A^*]_0 \frac{1-\beta}{exp(1/\tau_T) - \beta}\right)^2 \tag{3.5}$$

I_{th} is defined in Equation (3.6), as a function of the rate constants of first- and second-order annihilator triplet decay (k_T and k_{TTA}, respectively), the absorption cross-section of the sensitizer (α), and the sensitizer ground state concentration ($[^1S]_0$).

$$I_{th} = \frac{k_T^2}{2k_{TTA}\alpha[^1S]_0} \tag{3.6}$$

3.5 Microscopy

Although spectroscopic techniques served as the main tool of investigation for the experiments conducted in this thesis, optical microscopy was used in both **Paper I** and **Paper IV**. It is a powerful tool that in these two papers was used to study both fixed cells and microcapsules, and this section aims to give a brief explanation to the different microscopy techniques that were used.

Wide-field, and more specifically bright-field, microscopy involves illuminating the entire sample with light and capturing the entire field of view simultaneously. It is a fast imaging technique, where the light that passes directly through the sample produces a dark image of the sample against a bright background. Since the imaged samples in this thesis are fluorescent, they could also be imaged using

fluorescence microscopy. In fluorescence microscopy, the samples are illuminated with light of a wavelength that excites the fluorescent species, resulting in emission that can provide information of where the fluorescent species are located. Confocal microscopy is a fluorescence laser scanning technique. It enhances resolution and contrast by placing a pinhole in a conjugate plane to the sample, eliminating out-of-focus light. This allows for the imaging and scanning of thin optical sections within a sample, which can produce high-resolution, three-dimensional images.[80]

4

Intensity Modulation of a Turn-Off Mode Fluorescent DAE

Recalling the molecular photoswitches introduced in section 2.2.2, this chapter will focus on a photochromic molecule from the diarylethene (DAE) family. DAEs exhibiting fluorescence exclusively when in their open isomeric state, while remaining non-emissive in their closed configuration, are classified as turn-off mode DAEs.[34] Upon exposure to UV irradiation, the UV-induced fluorescence of the initial open-form diminishes due to the isomerization to DAEc by UV light. This chapter is based on **Paper I**[81] and employs an asymmetric DAE, denoted as Dasy,[82] with Figure 4.1 illustrating the structures of its open (Dasy(o)) and closed (Dasy(c)) isomers within an isomerization scheme. Dasy, a water-soluble derivative, demonstrates a significant fluorescence quantum yield of 0.21 in water for its open isomer. While there is another DAE derivative that possesses a fluorescence quantum yield similar to this value for its open isomer, its fluorescence cannot be entirely quenched upon UV light exposure due to that the open isomer is far from fully converted into the closed isomer at the photostationary state (PSS).[83] In contrast, Dasy can achieve nearly 100% conversion to Dasy(c) under UV light exposure.

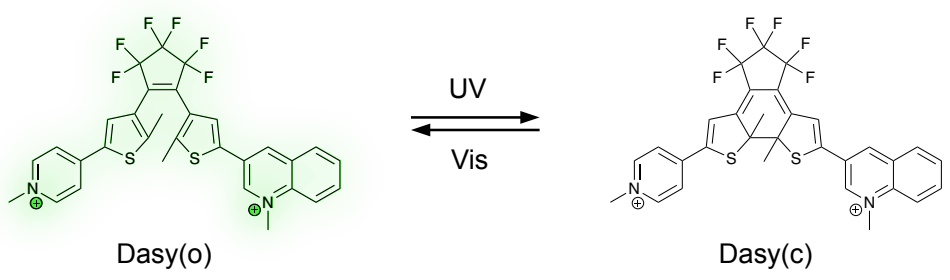

Figure 4.1: Structures and isomerization scheme of Dasy. UV light isomerizes the open isomer Dasy(o) to the closed isomer Dasy(c), and visible light is used to facilitate the reverse isomerization. The green glow on Dasy(o) is there to visualize its UV light induced fluorescence.

Figure 4.2 depicts the absorption spectra of Dasy(o) and Dasy(c), along with the fluorescence of Dasy(o) in aqueous solution. Dasy(o) exhibits its most red-shifted absorption band centered at 351 nm, primarily absorbing in the UV region. Dasy(c) on the other hand absorbs in the visible region as well, with an absorption band centered at 644 nm. The ring-closing reaction induced by 365 nm irradiation has an isomerization quantum yield of 0.44, and the ring-opening reaction induced by 523 nm irradiation has an isomerization quantum yield of 0.0033. As mentioned earlier, Dasy(o) exhibits pronounced fluorescence when exposed to UV light, displaying a peak emission at 511 nm.

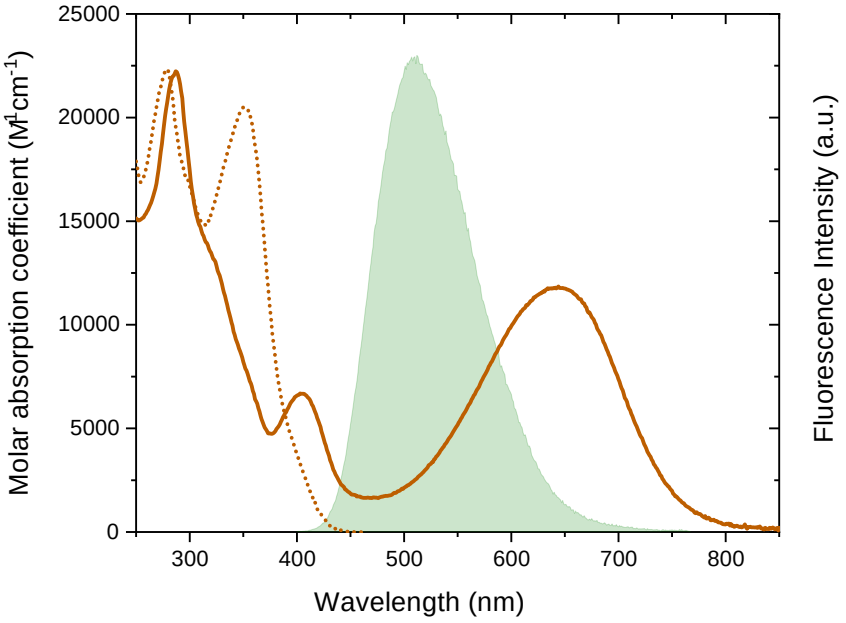

Figure 4.2: Absorption spectra of Dasy(o) (dotted brown line) and Dasy(c) (solid brown line) together with the emission spectrum of Dasy(o) (filled green) in water.

The distinctive attributes of Dasy, such as its water solubility, high fluorescence quantum yield in the colorless open form, and the capability to fully transition between open and closed isomers, position it as an excellent candidate for biological applications. In this project, the primary objective revolves around augmenting fluorescence microscopy contrast through rapid fluorescence modulation. A prevalent challenge in fluorescence microscopy pertains to discriminating desired fluorescence, typically stemming from synthetic fluorescent probes, from unwanted cellular autofluorescence. This dilemma reduces achievable contrast in fluorescence microscopy, since the background emission constrains the signal-to-background ratio. To discern desired fluorescence amidst bright backgrounds, modulation of

excitation light and the utilization of optical lock-in detection (OLID) can facilitate the capture of amplitude-modulated emission from fluorescent probes. This method proves effective if probe emission, but not autofluorescence, can be modulated. Prior examples have been confined to organic solvents[84,85] and necessitating extensive (synthetic) sample preparation due to multi-chromophoric systems,[84–89] limiting the bio-relevance and usability. With reported modulation frequencies below 1 Hz,[86–90] the acquisition times for these systems becomes unpractically long for the intended application. Marriott *et al.* pushed the field towards utilization in a cellular environment, using a spiropyran as the fluorescent probe.[90,91] Albeit showing a simpler and more bio-relevant system, it still suffers from a meager fluorescent quantum yield (around 0.01)[92] and poor photostability. With the spiropyran being fluorescent in its colorless open form, discerning the probe signals from background noise necessitates extensive data processing. Dasy addresses all these challenges, enabling modulation frequencies that markedly surpass previously reported frequencies.

4.1 Rapid Modulation

The amplitude modulation of Dasy(o) fluorescence involved continuous UV irradiation of an aqueous Dasy solution, with Dasy initially in its fluorescent Dasy(o) form, until reaching a PSS exclusively comprising Dasy(c), thereby extinguishing the initial fluorescence. Upon exposure to red light at this juncture, while maintaining the UV light, isomerization from Dasy(c) to Dasy(o) is induced. Consequently, at the new PSS resulting from simultaneous UV and red light irradiation, fluorescence is reactivated. Through sustained UV irradiation and modulation of the red light, the fluorescence of Dasy can be toggled on and off, as depicted schematically in Figure 4.3. Despite UV light triggering fluorescence, it is the modulation of light not absorbed by the fluorescent species that governs the fluorescence intensity. In Figure 4.3, A_m represents modulation amplitude, f_m denotes modulation frequency, and k_{obs} signifies the observed rate constant for attaining the PSS induced by simultaneous irradiation of Dasy(o) with UV and red light.

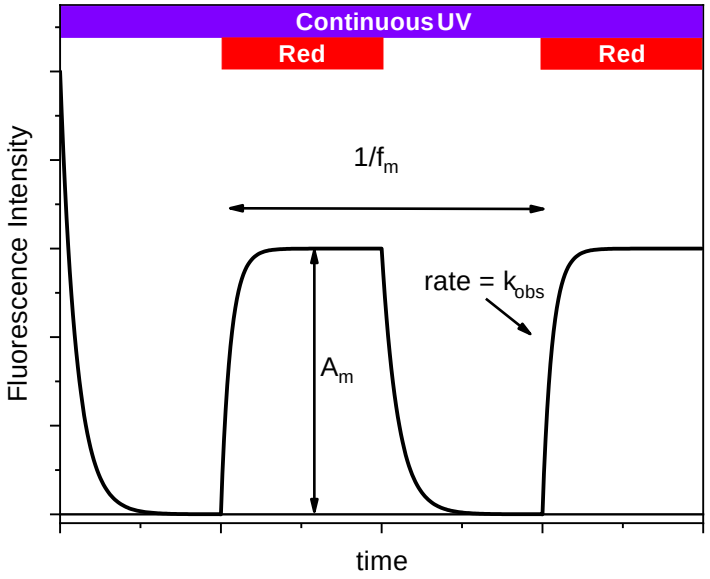

Figure 4.3: Schematic illustration of how Dasy is switched between the two photostationary states, when alternately irradiating the sample with only UV light and both UV and red light simultaneously. f_m is the modulation frequency, A_m is the modulation amplitude and k_{obs} is the observed rate constant for the process of reaching the photostationary state resulting from simultaneous irradiation with UV and red light. At the start of the experiment, Dasy is in its fluorescent Dasy(o) isomeric form.

An experimental demonstration of amplitude modulation of Dasy(o) fluorescence is illustrated in Figure 4.4, showcasing different modulation frequencies. In all instances, an aqueous solution of Dasy with a concentration of approximately 20 μM was subjected to continuous 365 nm UV light (∼30 mW) and square-wave modulated 660 nm red light (∼40 mW). Red light modulation was performed at increasing frequencies: 10 Hz (left), 105 Hz (middle), and 205 Hz (right). At low frequencies, the modulation amplitude remains constant across frequency variations, as irradiation durations suffice for complete isomerization between the two PSS. With further increases in f_m, there is an initial drastic decline in A_m, which stabilizes at higher modulation frequencies. This relationship between A_m and f_m is further elucidated in **Paper I**.

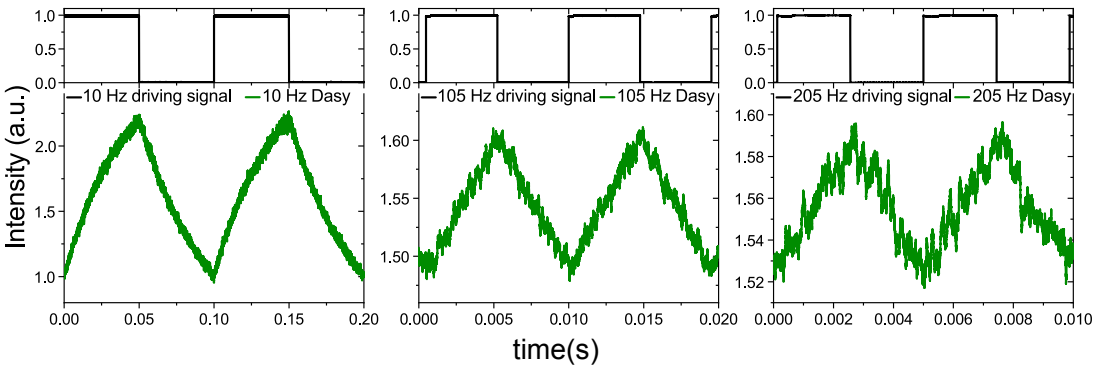

Figure 4.4: Amplitude modulation of Dasy in aqueous solution with modulation frequencies of 10 Hz (left), 105 Hz (middle) and 205 Hz (right). The samples were under constant 365 nm (∼30 mW) irradiation, and the 660 nm laser (∼40 mW) was modulated at different frequencies (black lines) inducing the fluorescence modulation of Dasy recorded at 500 nm (green lines).

4.2 Background Removal

OLID stands as a method capable of discerning an alternating signal with a fixed frequency amidst a consistent background, as previously noted for its potential in enhancing contrast in fluorescence microscopy. Following the demonstration of rapid amplitude modulation of Dasy(o) fluorescence, the subsequent endeavor aimed to differentiate Dasy emission from a luminous background. This endeavor entailed the utilization of a 450 nm light source, characterized by its spectral profile depicted in Figure 4.5 (purple line), to act as a background signal emulating e.g. cell autofluorescence. A steady-state emission spectrum was captured from Dasy(o) continuously excited by 365 nm light, while concurrently exposing the detector to the 450 nm light source (brown line). Evidently, the contribution of the 450 nm light source dominates this spectrum. A comparative spectrum was then acquired with Dasy(o) and the 450 nm light source, this time employing OLID for signal capture. Dasy underwent continuous irradiation by 365 nm light, alongside 660 nm light modulated at a frequency of 10 Hz. The lock-in amplifier was finely tuned to detect a 10 Hz signal, while the detector scanned the identical wavelength region as during the steady-state measurement. The resulting recording, depicted as a green filled spectrum in Figure 4.5, distinctly reveals the complete filtration of continuous bright background light (the 450 nm light source), leaving only Dasy(o) emission in the spectrum (cf. Figure 4.2).

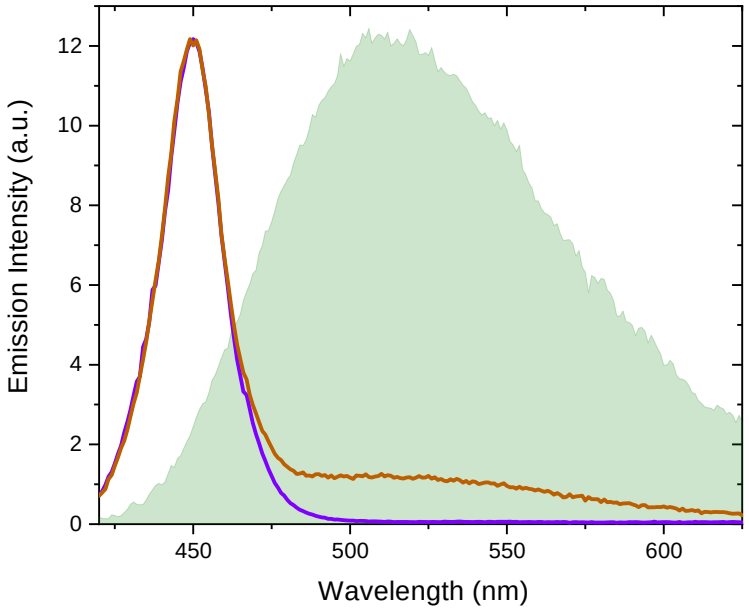

Figure 4.5: Spectral profile of the 450 nm light source (purple line), steady-state emission spectrum of Dasy(o) fluorescence together with the 450 nm light source (brown line), together with an amplitude-modulated spectrum of Dasy(o) + the 450 nm light source under 10 Hz modulation of the 660 nm laser and continuous 365 nm irradiation (green filled). All spectra are normalized to a common maximum value.

We have effectively demonstrated the capability of rapidly modulating Dasy fluorescence in aqueous solution, coupled with the facile extraction of the signal from a luminous background using OLID. To further underscore Dasy's suitability for contrast enhancement in fluorescence microscopy, **Paper I** also encompasses measurements involving Dasy(o) added to a mouse fibroblast cell line. These findings illustrate the detectability of amplitude-modulated Dasy fluorescence within a cellular milieu, characterized by excellent fatigue resistance. Additional insights into the cell studies are elaborated upon in **Paper I**.

5

All-Visible-Light Switching of DAEs Through Triplet Sensitization

Promoting ring-closing reactions of DAEs typically necessitates UV light, introducing drawbacks such as photodegradation and limited tissue penetration.[8,9] Various approaches have therefore been explored to achieve all-visible-light switching of DAEs.[93,94] One strategy involves chemically extending the π conjugation, requiring intricate synthesis.[95,96] Alternatively, utilizing upconverting nanoparticles to generate UV light from visible or near-IR light has, instead, resulted in low photoisomerization quantum yields.[97,98] Another method involves driving the cyclization reaction along the triplet manifold through sensitization, rather than singlet excitation of the open isomers. This process requires less energy since the first triplet excited state of the DAEs is lower in energy than the first singlet excited state, making it feasible to use light of longer wavelengths than direct UV excitation. The utilization of visible light enhances the fatigue resistance of repeated DAE isomerization, as photodegradation predominantly occurs on the singlet manifold.[99,100] There has been examples of employing TET from molecular triplet sensitizers,[45–49] yet this approach suffers from constraints in molecular design, low molar absorptivities, and high sensitivity to oxygen. In the study conducted in **Paper II**[17] and summarized in this chapter, we propose a general approach to all-visible-light switching of DAEs that maintains high photoisomerization efficiencies and excellent fatigue resistance compared to direct UV isomerization.

Semiconducting nanocrystals (NCs), or quantum dots, are quantum confined inorganic crystals. They possess several properties making them suitable for photochemical applications,[101–103] including high molar absorptivities and often stable and high photoluminescence quantum yields.[104] By adjusting synthesis conditions such as reaction temperature and time, the size of the NCs can be readily controlled.[105,106] As the absorption and emission profiles strongly depend on the size of the NCs, they can be tailored to meet various energetic requirements. NCs

exhibit strong spin-orbit coupling, resulting in a minimal energy difference between the first singlet and triplet excited states. Despite these favorable properties for triplet sensitization, NCs have very short triplet lifetimes, limiting their use in diffusion-controlled processes. Hence, we herein attach phenanthrene-3-carboxylic acid (3-PCA) molecules to the surface of cadmium sulfide (CdS) NCs to act as triplet mediators, which can harvest the NC triplets as long-lived molecular triplets.[107–109] A schematic representation of the CdS NC/3-PCA hybrid is depicted in Figure 5.1, along with the molecular structure of 3-PCA.

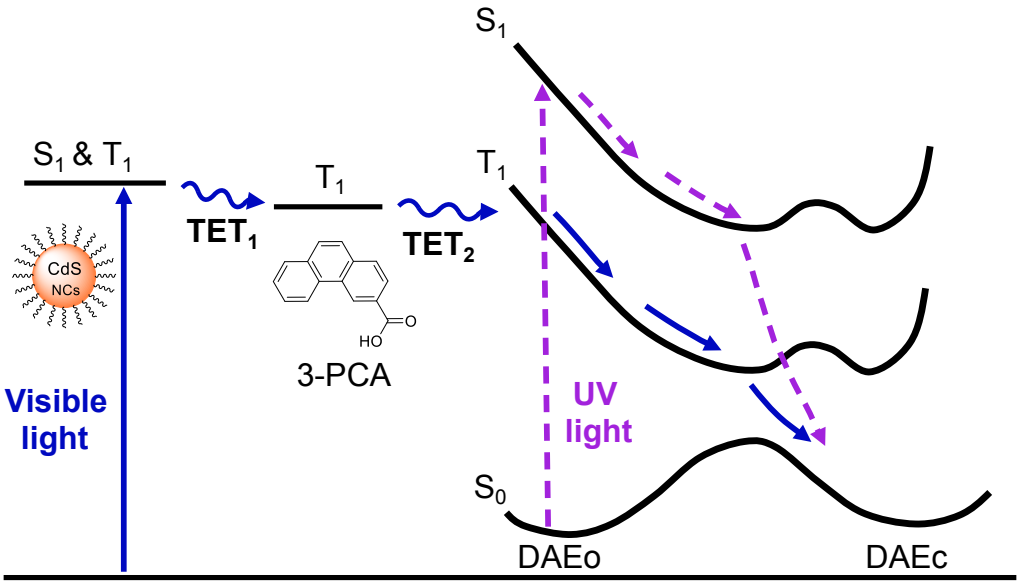

Figure 5.1: Schematic illustration showing the photoisomerization from DAEo to DAEc. The route induced by visible light irradiation *via* two triplet energy transfer steps (TET_1 and TET_2) from CdS NCs and 3-PCA is shown as blue arrows, and direct UV induced isomerization is shown as dashed purple arrows for comparison.

The visible light-induced isomerization from DAEo to DAEc utilizing the CdS NCs/3-PCA hybrid triplet sensitizers is depicted in Figure 5.1 by blue arrows. Visible light excites the CdS NCs, followed by two triplet energy transfer steps (TET_1 and TET_2), first to 3-PCA and then to DAEo, resulting in isomerization to DAEc along the triplet manifold. For comparison, direct UV isomerization along the singlet manifold of the DAE is indicated by purple dashed arrows. To demonstrate the versatility of our approach in achieving all-visible-light-induced isomerization of DAEs, we employ four DAE derivatives denoted as DAE1, DAE2, DAE3, and DAE4. Their structures and isomerization schemes are depicted in Figure 5.2. DAE1 and DAE2 are sensitized using CdS NCs with an absorption peak at 405 nm, denoted as CdS 405 in the figure. The remaining two DAEs are sensitized using CdS NCs with absorption peaks at 425 nm and 450 nm, and three

sizes of CdS NCs are synthesized to match the desired irradiation wavelength for inducing ring-closing reactions at 405 nm, 425 nm, and 445 nm, respectively. A wavelength of 590 nm is employed to facilitate the reverse isomerization for all four DAEs.

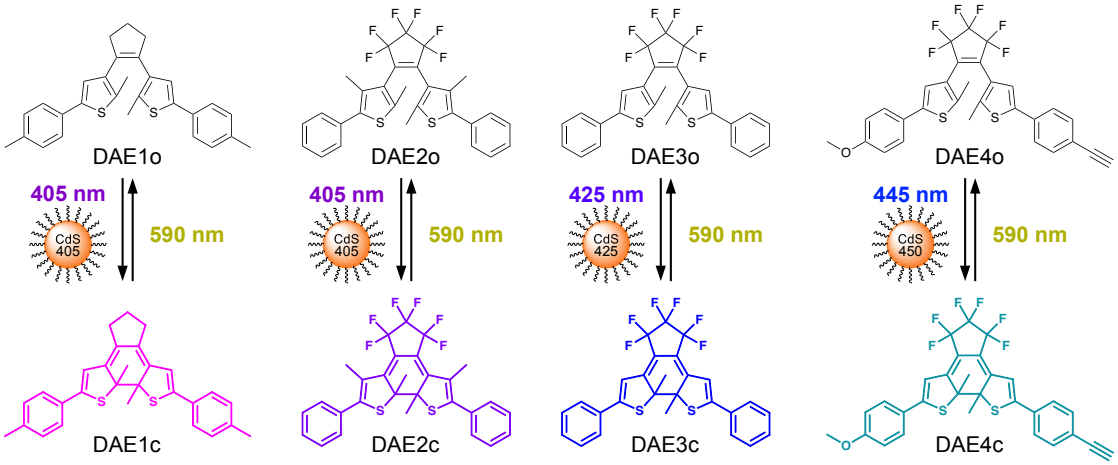

Figure 5.2: Structures and isomerization schemes of the four DAEs. CdS NCs with varying absorption bands are used to facilitate visible light (405 nm, 425 nm, and 445 nm) induced isomerization from DAEo to DAEc, and 590 nm light is used to facilitate the reverse isomerization.

5.1 All-Visible-Light Switching

In pursuit of achieving all-visible-light switching of the DAEs and confirming the pivotal role of TET in driving the photoisomerization, we synthesized CdS NCs to match the absorption bands of the photochromic molecules' transparent windows, as detailed in prior studies.[110,111] 3-PCA was linked to the CdS NC surface via its carboxylic acid functional group. Since the mediator is transparent for wavelengths longer than 370 nm, it will absorb none of the visible light sources used for inducing sensitized ring-closing reactions. The mixture comprised 0.3 or 0.5 μM CdS together with 100 μM 3-PCA and 50 μM of the respective DAEs in their open as-synthesized form. Absorption spectra of the four DAEo mixtures in deaerated toluene are illustrated in Figure 5.3 (green lines). Subsequent irradiation with light matching the CdS NC absorption bands (405 nm for DAE1 and DAE2, 425 nm for DAE3, and 445 nm for DAE4) facilitated the formation of DAEc (purple lines).

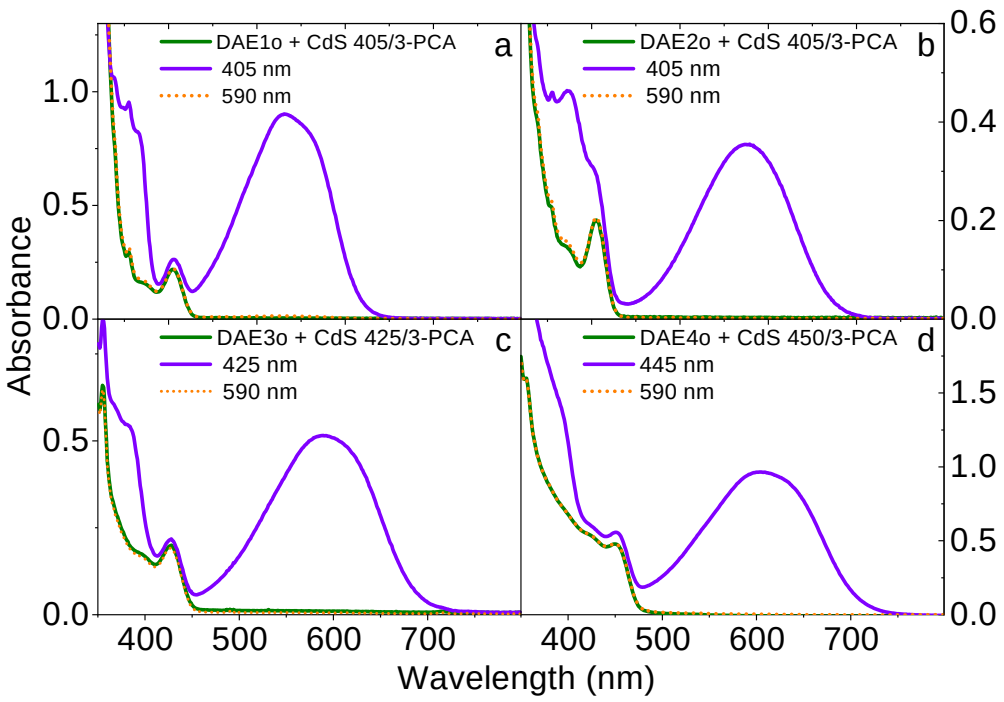

Figure 5.3: Absorption spectra of solutions containing the DAE derivatives (50 μM of a) DAE1, b) DAE2, c) DAE3, and d) DAE4), CdS NCs (0.5 μM CdS 405 in a and b, 0.3 μM CdS 425 in c, and 0.5 μM CdS 450 in d) and 3-PCA (100 μM) in deareated toluene. Spectra are recorded for the open isomers before (green lines) and after irradiation of 405 nm, 425 nm, and 445 nm light, respectively (120 s, purple lines), and then after subsequent 590 nm light irradiation (90 s, orange dotted lines).

Upon 405 nm irradiation of the DAE1o sample, a 94% conversion to the closed isomer was observed at the PSS (see Figure 5.3a), same as the conversion reported for UV irradiation.[100] The photocyclization (ring-closing) quantum yield was determined to be 35%, close to that reported for direct 313 nm UV light irradiation (43%[100]). However, the conversion of DAE2 using 405 nm light was lower than that reported for 313 nm irradiation (58% versus 79%[112]), attributed to the larger spectral overlap between DAE2c absorption and the excitation light. This overlap causes competition between the triplet-mediated ring-closing reaction and direct ring-opening over the singlet manifold. Conversely, the photocyclization quantum yield under 405 nm for the DAE2 mixture matched that of 313 nm UV light isomerization (39%, compared to the previously reported 46%[112]). Figures 5.3c and 5.3d depict the successful isomerization of DAE3 and DAE4 to their respective closed form isomers using our approach. Subsequently, all four DAEs revert to their open form isomers upon 590 nm irradiation (orange dotted lines).

UV light triggers the formation of annulated byproducts of the DAEs,[99,100] as evidenced by the reduced absorbance at 530 nm of DAE1 recorded over time (see Figure 5.4). The left panel displays the results of eight irradiation cycles of 405 nm and 590 nm light for the mixture of DAE1 and CdS 405/3-PCA hybrids (black), alongside corresponding irradiation cycles using 302 nm and 590 nm light irradiation on DAE1 alone (red). Notably, the fatigue resistance is superior for all-visible-light switching of the DAE1 mixture. Note that the lines connecting the measured absorbance values marked as squares serve as a visual guide for readers to track the irradiation cycles. Another comparison demonstrating improved fatigue resistance when using visible instead of UV light is illustrated in the right panel. Here, the 530 nm absorbance of DAE1 is recorded over time, starting with only DAE1o isomers in the samples. The mixture is irradiated with 405 nm light (black), and DAE1 alone is irradiated with 302 nm light (red).

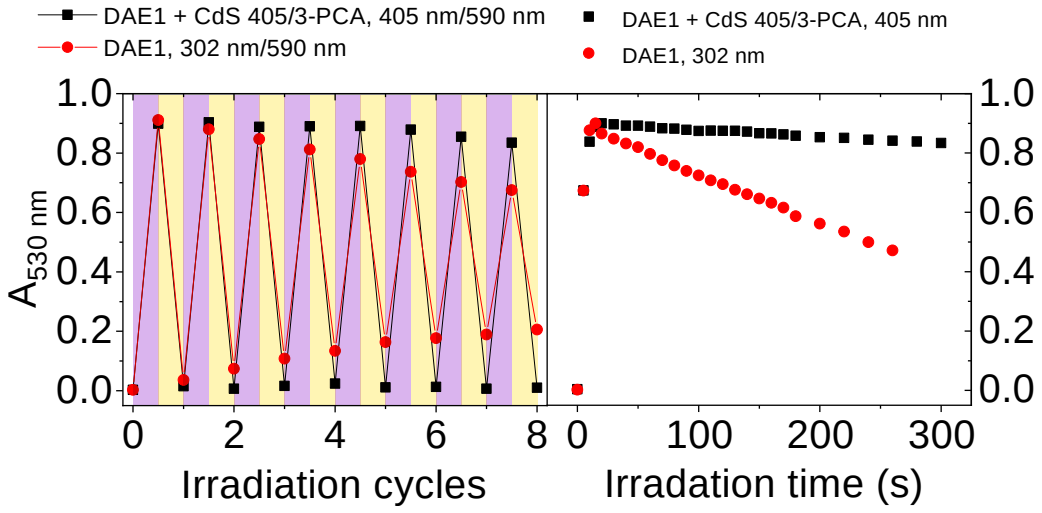

Figure 5.4: Photoswitching fatigue measurements. **Left:** Absorbance of DAE1 at 530 nm recorded over eight irradiation cycles of 405 nm and 590 nm light for the DAE1 + CdS 405/3-PCA mixture (black), and for DAE1 alone using 302 nm and 590 nm light (red). **Right:** Absorbance of DAE1 at 530 nm recorded over time for the mixture irradiated with continuous 405 nm light (black), and for DAE1 alone irradiated with continuous 302 nm light (red). Both starting with DAE1o.

5.2 Investigation of the Triplet Sensitization Process

The efficiency of the TET_1 process from CdS 405 to 3-PCA was found to be near-unity, standing at 91%, with comprehensive details available in the Supporting Information of **Paper II**. Additionally, specifics concerning the triplet energies of the compounds are also given in the paper. Notably, a peculiar observation arises

regarding the triplet energies: while the triplet energy of DAE1o is marginally lower than that of 3-PCA (2.5 eV[100] versus 2.6 eV[109]), the opposite holds for DAE2o, which is estimated to possess a triplet energy of 2.8 eV. According to the Sandros equation,[113] albeit slower, endothermic TET can still occur to DAE2o.

Nanosecond transient absorption spectroscopy (ns-TA) was employed to investigate the TET_2 process by adding DAE1 and DAE2 to solutions containing 1.5 μM CdS 405 and an excess of 300 μM 3-PCA in deoxygenated toluene, ensuring the formation of triplet excited 3-PCA via TET_1. A 415 nm pulsed laser (2.0 mJ, 10 ns) served as the excitation source for the DAE1 measurement, while the DAE2 sample was excited with a 410 nm pulsed laser. The TA signal was recorded at 470 nm and 450 nm, respectively, for DAE1 and DAE2 (top figures in Figure 5.5), both wavelengths lying within the broad positive absorption band of the 3-PCA triplet state.[109] Initially, both measurements exhibit a rise in the TA signal, attributed to the formation of triplet excited 3-PCA. Subsequently, in the absence of DAE derivatives, the triplet signal of 3-PCA decays monoexponentially with a lifetime of 22 μs. This lifetime is shortened upon the addition of DAE1 and DAE2, as the 3-PCA triplet energy is transferred to the DAE derivatives through TET_2. DAE1 and DAE2 can be viewed as triplet quenchers in this experiment, and this phenomenon can be elucidated using the Stern-Volmer equation as defined in Equation (3.3).

Stern-Volmer plots for DAE1 (left) and DAE2 (right) are presented in the lower portion of Figure 5.5, alongside their respective linear fits (depicted by red lines). The fitting process yielded k_q values of $1.4 \cdot 10^9$ $M^{-1}s^{-1}$ for DAE1 and $2.7 \cdot 10^7$ $M^{-1}s^{-1}$ for DAE2. The value for DAE1 falls within the expected magnitude for an efficient diffusion-controlled process, while the k_q for DAE2 is almost two orders of magnitude smaller. This observation aligns with the previous discussion concerning the triplet energy of DAE2o, which is somewhat higher than that of 3-PCA, resulting in a slower endothermic TET_2 process.

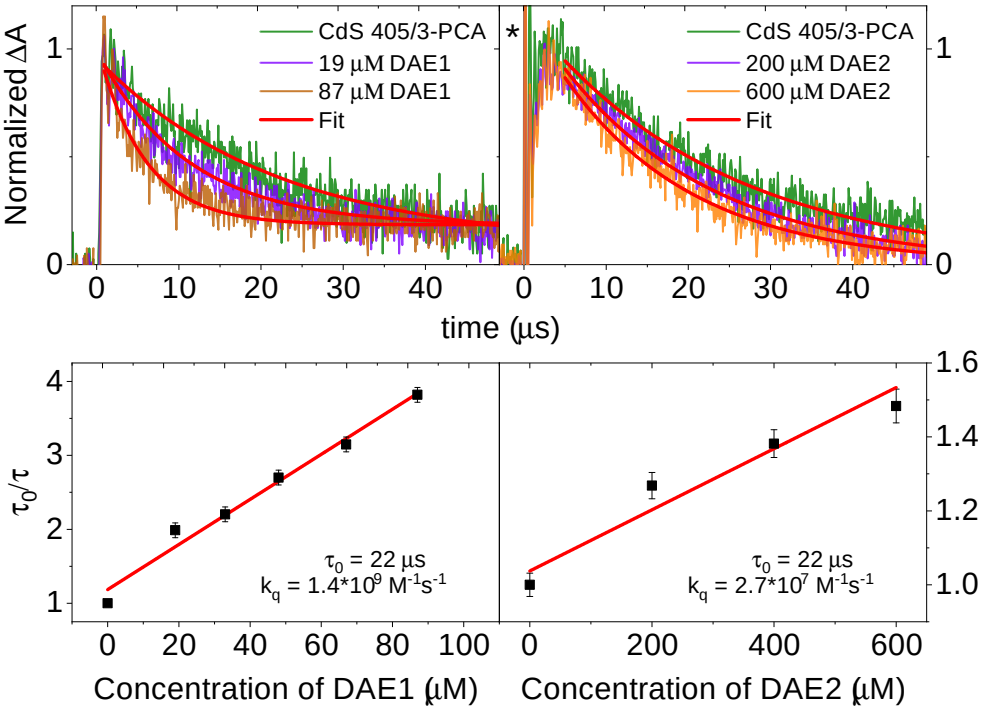

Figure 5.5: DAE quenching of the CdS 405/3-PCA hybrid triplet state. **Top figures:** Time-resolved transient absorption decays of CdS 405/3-PCA (1.5 μM CdS 405 and 300 μM 3-PCA) in deareated toluene, recorded at 470 nm upon 415 nm pulsed excitation adding DAE1 (left) and recorded at 450 nm upon 410 nm pulsed excitation adding DAE2 (right). *The initial rise in the DAE2 traces is due to laser scattering. **Bottom figures:** Stern-Volmer plots with linear fits (red lines) for DAE1 (left) and DAE2 (right) quenching of the CdS 405/3-PCA triplet lifetime.

5.3 Solid State Switching

We have demonstrated that our proposed system offers a universal method for achieving all-visible-light isomerization across various DAE derivatives. The photoisomerization quantum yields are comparable to those achieved using UV light, and cyclization via the triplet manifold exhibits enhanced fatigue resistance. Moreover, as depicted in Figure 5.6, the CdS NCs/3-PCA hybrids perform admirably in the solid state as well. The solid state experiments involved saturating a filter paper with a solution containing CdS 405, 3-PCA, and the colorless DAE2o in toluene, followed by solvent evaporation. Subsequent irradiation with 405 nm and 590 nm light, coupled with the use of masks, induces color and pattern alterations on the paper, as depicted in the figure, facilitating the transition of DAE2 between the colorless DAE2o and the colored DAE2c states. Further elucidation is provided in **Paper II**.

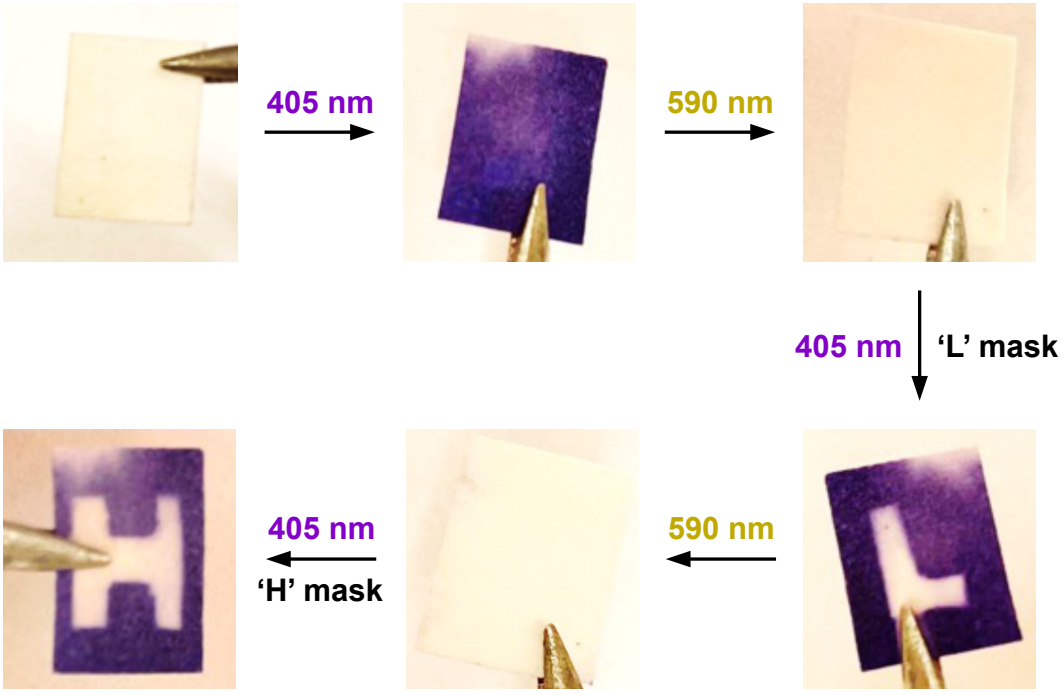

Figure 5.6: Photographs showing all-visible-light-switching of DAE2 in the solid state. A filter paper was soaked in a solution containing DAE2, CdS 405 and 3-PCA. After solvent evaporation, the color (white and purple) and pattern (letters 'L' and 'H') were changed by subsequently irradiating the filter paper with 405 nm and 590 nm light. This was all done in a normal atmospheric environment.

6

Controlling Photochemistry Using TTA-UC

In the preceding chapter, the employment of triplet sensitization enabled the utilization of visible light to catalyze ring-closing reactions for DAEs, traditionally necessitating UV light. However, a limitation of employing triplet sensitization in driving photochemical reactions is the requirement for the sensitizer to be in close proximity to the photochemical reactant.[45–49] This poses no issue if no subsequent separation step between the sensitizer and the photochemical products is needed, and if both components share the same phase, such as the liquid solutions employed in the previous chapter. In **Paper III**[114] and **Paper IV**, we adopt a different strategy by employing TTA-UC[21–23] to facilitate the isomerization of DAEs and a spiropyran using light with lower energy than that absorbed by the photoswitch. This enables us to maintain physical separation between the upconversion (UC) solution and the photoreactant solution, either using separate chambers (**Paper III**) or encapsulating the TTA-UC solution in microcapsules (**Paper IV**). TTA-UC has previously demonstrated efficacy in facilitating various photochemical reactions,[61–67,115–120] including photoisomerization.[121,122]

6.1 Single Wavelength Control of DAEs using TTA-UC

In **Paper III**, we utilize a single green light source to both instigate reversible isomerization and trigger fluorescence from the closed isomer among a set of DAE derivatives. The findings pertaining to the derivatives labeled as DAE1, DAE2, and DAE3 (distinct from those mentioned in Chapter 5) are presented herein. While both the ring-opening reaction and the induction of fluorescence from DAEc can be directly managed using green light, the ring-closing reaction necessitates higher energy light, typically in the UV region. To drive this latter process with a green light source, a well-established green-to-blue TTA-UC pair composed of platinum octaethylporphyrin (PtOEP) as the sensitizer and 9,10-diphenylanthracene

(DPA) as the annihilator is employed. The molecular structures of PtOEP and DPA are illustrated in the upper panel of Figure 6.1, while the structures and isomerization scheme between DAEo and DAEc of the three DAE derivatives are depicted in the lower panel of the same figure.

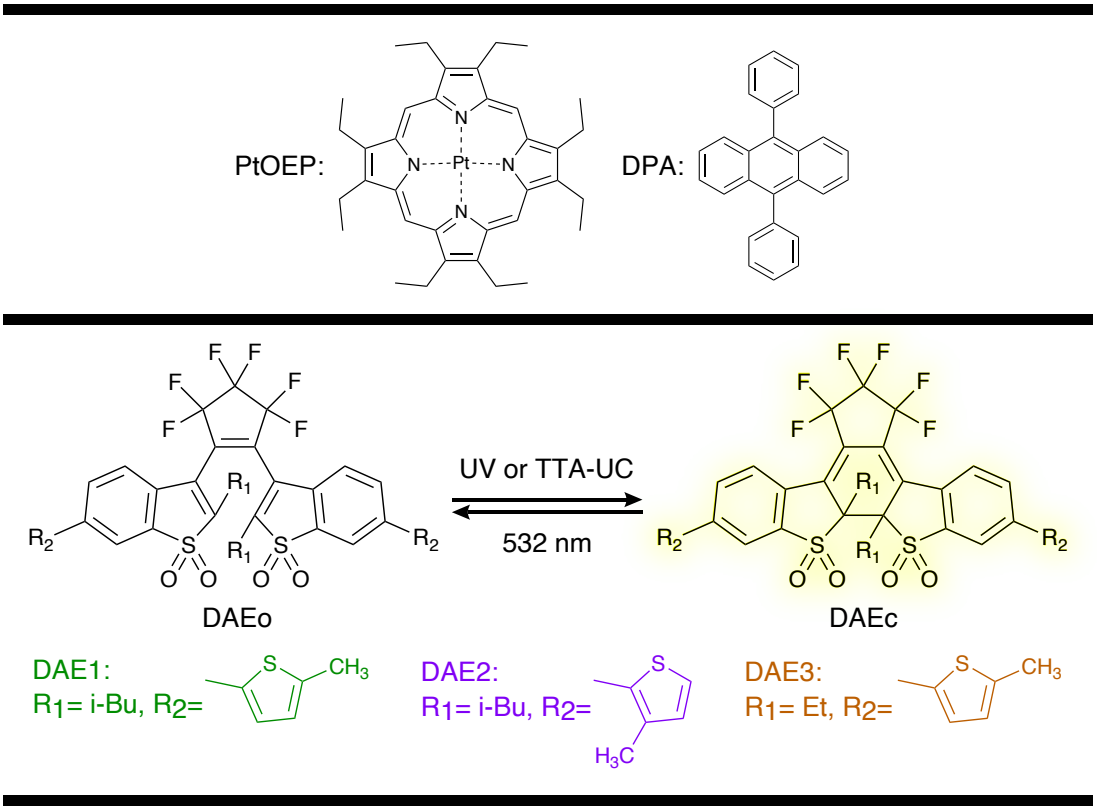

Figure 6.1: Top panel: Structures of PtOEP and DPA. **Bottom panel:** Structures and isomerization scheme of the three DAEs: DAE1 (green), DAE2 (purple), and DAE3 (brown). UV light or upconverted (TTA-UC) light can be used to isomerize from DAEo to DAEc, and 532 nm light is used to facilitate the reverse isomerization. The yellow glow on DAEc is there to visualize its green light induced fluorescence.

To maintain physical separation between the DAE solution and the UC solution, we employ a two-chamber quartz cuvette, as illustrated for DAE2 in the photographs in Figure 6.2. When initiating the isomerization from DAEc to DAEo, 532 nm light is directed solely through the DAE chamber. Conversely, the rightmost image depicts laser irradiation (indicated by a green arrow) when commencing with DAEo in the DAE chamber, triggering the ring-closing reaction, and subsequently initiating the fluorescence of DAEc (experimentally observed in Figure 6.4). Throughout this experiment, the laser is directed through the DAE chamber, which initially does not absorb any of the incoming 532 nm laser light. The green light then reaches the UC chamber, prepared with concentrations (10 mM DPA and 0.5 mM PtOEP in toluene) ensuring 99% attenuation of the 532

nm light within the first millimeter of the UC chamber. This setup ensures that most of the TTA-UC occurs proximate to the quartz wall separating the two solutions, minimizing secondary inner-filter effects of the blue UC fluorescence before reaching the photochromic molecules.

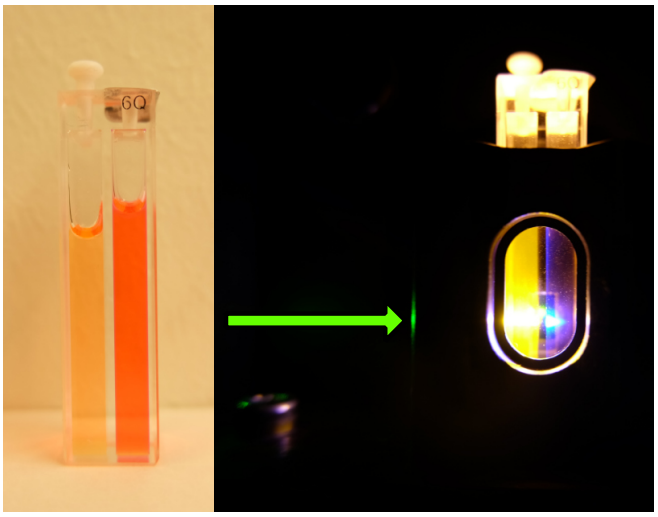

Figure 6.2: Photographs showing two-chamber cuvettes containing DAE2 (left chamber) and the PtOEP/DPA upconversion solution (right chamber), both in toluene. The photograph to the left shows the cuvette in ambient light, and the photograph to the right shows the cuvette in the dark under 532 nm laser irradiation from the left (indicated by the green arrow) through the DAE2 chamber into the upconversion chamber.

Absorption spectra of DAEo and DAEc for the three DAE derivatives are depicted in Figure 6.3, alongside normalized DAEc fluorescence, and upconverted DPA emission measured semi-front-face in the two-chamber cuvette (refer to **Paper III** for experimental details). Similar to the DAE derivatives discussed in Chapters 4 and 5, DAEo predominantly absorbs UV light, while DAEc also exhibits absorption in the visible region. DAEo is virtually non-emissive, while DAEc showcases strong fluorescence for all three DAE derivatives with fluorescence quantum yields of 0.75,[123] 0.83, and 0.78,[124] for DAE1, DAE2, and DAE3, respectively. The intense yellow fluorescence from DAE2c is observable in the rightmost photograph in Figure 6.2. A slight spectral overlap exists between the DAEo absorption and the upconverted emission (see Figure 6.3), enabling the utilization of upconverted photons to enable the ring-closing reaction. Despite a more substantial spectral overlap between the upconverted emission and the DAEc absorption, we can still induce isomerization from DAEo to DAEc. This observation arises from the isomerization quantum yields of the ring-closing reactions (0.30,[123] 0.39, and 0.23[124]), which are several orders of magnitude larger than those of the ring-opening reactions ($3.4{\cdot}10^{-5}$,[123] $2.4{\cdot}10^{-4}$, and $<1.0{\cdot}10^{-5}$,[124]) for these derivatives.

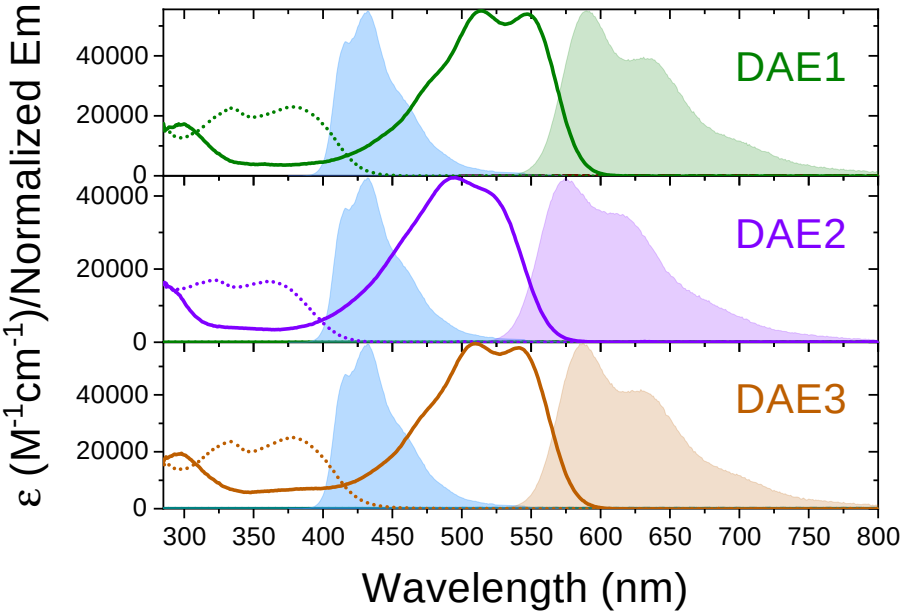

Figure 6.3: Absorption spectra of DAE1o, DAE2o, and DAE3o (dotted lines) and DAE1c, DAE2c, and DAE3c (solid lines) together with the emission spectra of DAE1c, DAE2c, and DAE3c (filled right-most spectra) and the upconverted DPA emission as measured in the two-chamber cuvette setup (blue filled spectra). All spectra are measured in toluene, and the upconversion sample was prepared in an oxygen free environment.

6.1.1 Green Light Induced Isomerization and Fluorescence

Recording the DAEc fluorescence provided evidence of the capability for TTA-UC to initiate the ring-closing reaction. Illustrated in Figure 6.4 is the temporal profile of DAEc fluorescence, measured at the emission peaks in toluene (592 nm, 578 nm, and 592 nm) for DAE1, DAE2, and DAE3. Initially, the DAEs existed in their as-synthesized non-fluorescent open forms. At the onset of the measurement, a 532 nm laser was activated, resulting in an immediate surge in the emission signal when the UC solution was present in the adjacent cuvette chamber (depicted in green, purple, and brown, respectively), while no significant emission signal was observed with toluene alone in the adjacent chamber (indicated in red). This observation distinctly illustrates that the green-to-blue upconversion instigates the ring-closing reaction. Over time, the fluorescence intensity levels out at the PSS achieved when the DAE chamber is concurrently exposed to 532 nm irradiation and upconverted photons.

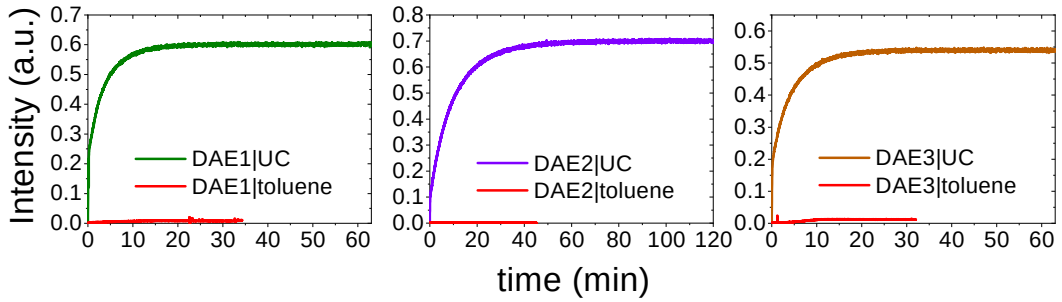

Figure 6.4: DAEc fluorescence measured at the respective emission peaks of DAE1c, DAE2c, and DAE3c (592 nm, 578 nm, and 592 nm) over time, measured in the two-chamber cuvette with (green, purple, and brown, respectively) and without (red) upconversion solution in the other cuvette chamber. Initially, the DAE chamber contained only the non-fluorescent DAEo isomer. At time zero the 532 nm laser was turned on, resulting in DAEc formation and subsequent fluorescence in the presence of upconversion solution. In the absence of upconversion solution, no significant DAEc fluorescence was detected indicating that no DAEc was formed.

Our two-chamber cuvette configuration affords us the ability to selectively activate various photophysical processes using the 532 nm laser by irradiating different regions of the cuvette. Figure 6.5 shows the resulting absorption spectra when only the DAE chamber underwent irradiation, with DAE2 being chosen to exemplify this change. Initially, DAE2 was in its closed isomeric form, exhibiting pronounced absorption at 532 nm. Absorption spectra resulting from 1, 3, and 5 hours of 532 nm irradiation are presented alongside spectra of DAE2o and DAE2c. It becomes evident that the isomerization from DAE2c to DAE2o can also be initiated by the same light source employed to initiate the ring-closing reaction and elicit fluorescence from DAE2c. After 5 hours, nearly all DAE2c had isomerized to DAE2o.

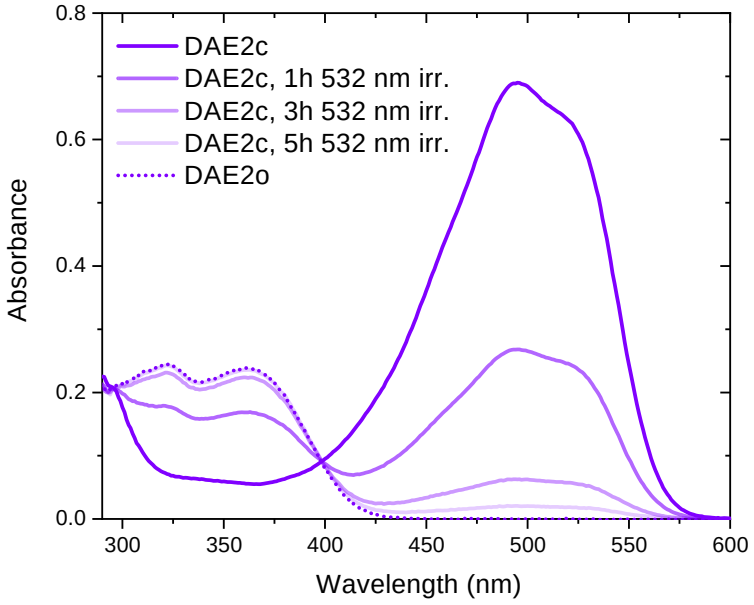

Figure 6.5: Absorption spectra of DAE2c (solid purple line) and DAE2o (dotted purple line), together with the resulting spectra of DAE2c after 1, 3 and 5 hours (more and more transparent purple) of 532 nm laser irradiation only through the DAE2 chamber. Hence, no TTA-UC occurred and therefore only the ring-opening reaction was triggered by the green light.

6.1.2 Performance of the TTA-UC-Driven Isomerization

Finally, the efficacy of TTA-UC-driven isomerization from DAE2o to DAE2c was compared with direct 365 nm LED-driven isomerization, as depicted in Figure 6.6. This comparison entailed preparing highly concentrated DAE2 solutions (approximately 800 μM) in one cuvette chamber, while filling the other chamber with either UC solution or toluene. Detailed insights into this comparative analysis are elucidated in **Paper III**. In essence, the high DAE2 concentration facilitated an approximation of total absorption of both the upconverted and the 365 nm photons. Linear fitting of the initial zeroth-order kinetics, coupled with the disparity in irradiation power between the two light sources (16.2 mW for the 532 nm laser and 0.21 mW for the 365 nm LED), revealed that direct 365 nm LED-driven isomerization outperformed TTA-UC-driven isomerization by 140 times. This difference can be attributed to various loss factors, including the inadequate spectral overlap of DAE2o absorption and upconverted emission, angular dispersion of upconverted photons, and the observed upconversion efficiency, which were estimated to be 24%, 50%, and 6%, respectively, in our setup. With further refinement of the proposed system, most of these loss factors could be mitigated.

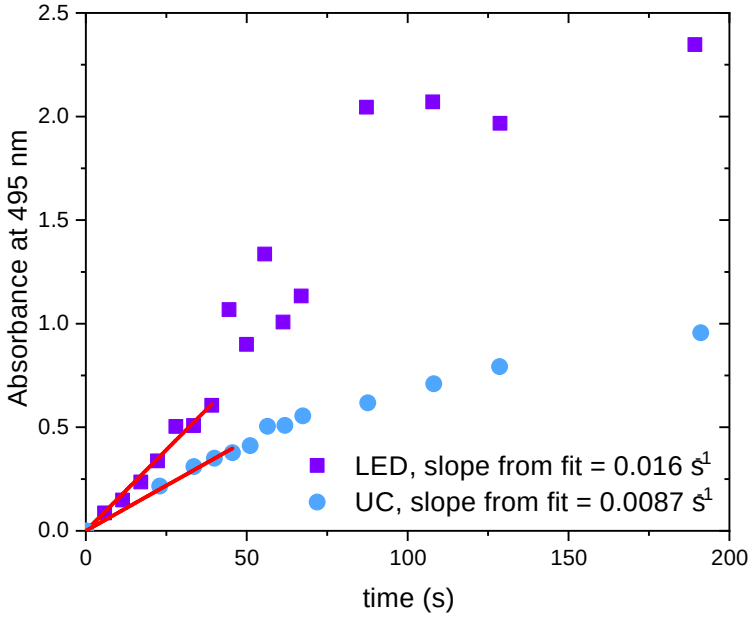

Figure 6.6: Comparison of the absorbance at the 495 nm centered DAE2c peak recorded over time during isomerization from DAE2o when using either a 365 nm LED (purple squares) or TTA-UC (blue circles), together with linear fits (red lines) of the initial absorbance change.

This investigation underscores the feasibility of employing a single green light source to facilitate both reversible photoisomerization of three DAE derivatives and induce fluorescence of DAEc through green-to-blue TTA-UC. This was achieved within a straightforward and adaptable experimental framework, where the triggered process could be selected by simply irradiating different segments of the sample. The physical separation between the UC and DAE solutions enabled characterization of the two solutions both individually and concurrently. Moreover, this physical segregation obviates the need for additional separation procedures, while allowing for facile adjustment of concentrations and solvents in the respective cuvette chambers.

6.2 TTA-UC in Microcapsules for Control of SP/MC Isomerization

In **Paper IV**, we investigate the optimization of TTA-UC for photochemical applications by encapsulating the upconversion system within microcapsules, maintaining the high local concentration of TTA-UC chromophores while minimizing

re-absorption losses. An investigation into previous encapsulation strategies reveals diverse examples, including different types of nanoparticles,[67,68,70,72,74,125–127] micelles,[71,73] and microcapsules,.[69,128] This study aims to address current challenges by developing a two-phase system of microcapsules meeting specific criteria: simple formulation procedures, ease of separation, non-toxicity, and water solubility. Furthermore, the utility of this approach is demonstrated by incorporating a spiropyran/merocyanine photoacid[41] into the continuous water solution, enhancing an isomerization/deprotonation reaction using upconverted photons. The core-shell microcapsules, fabricated via internal phase separation within an oil-water emulsion,[75,76] with an average diameter of 10 µm dispersed in water (Figure 6.7a). Although volatile organic solvents like toluene are commonly employed for TTA-UC, they are not feasible as core material for our microcapsules. Instead, glyceryl trioctanoate serves as the TTA-UC solvent making up the microcapsule core, surrounded by a poly(D,L-lactide-co-glycolide) (PLGA) polymer shell. These microcapsules, repurposed from controlled release applications,[76,129–131] utilizes platinum octaethylporphyrin (PtOEP) as the primary sensitizer and the analogous zinc octaethylporphyrin (ZnOEP) in certain microscopy studies. For the annihilator, 9,10-bis[(triisopropylsilyl)ethynyl]anthracene (TIPS-An) is employed, enabling green-to-blue TTA-UC within the microcapsule system. The core-shell structure together with the TTA-UC chromophore structures are shown in Figure 6.7b. Furthermore, as illustrated in Figure 6.7c, the upconverted blue light generated within these microcapsules serves as a pivotal agent in enhancing the photoisomerization and deprotonation process from the protonated merocyanine (MCH) to the deprotonated spiropyran (SP) form of the photoacid, highlighting the versatility and efficacy of the encapsulation approach in driving photochemical transformations.

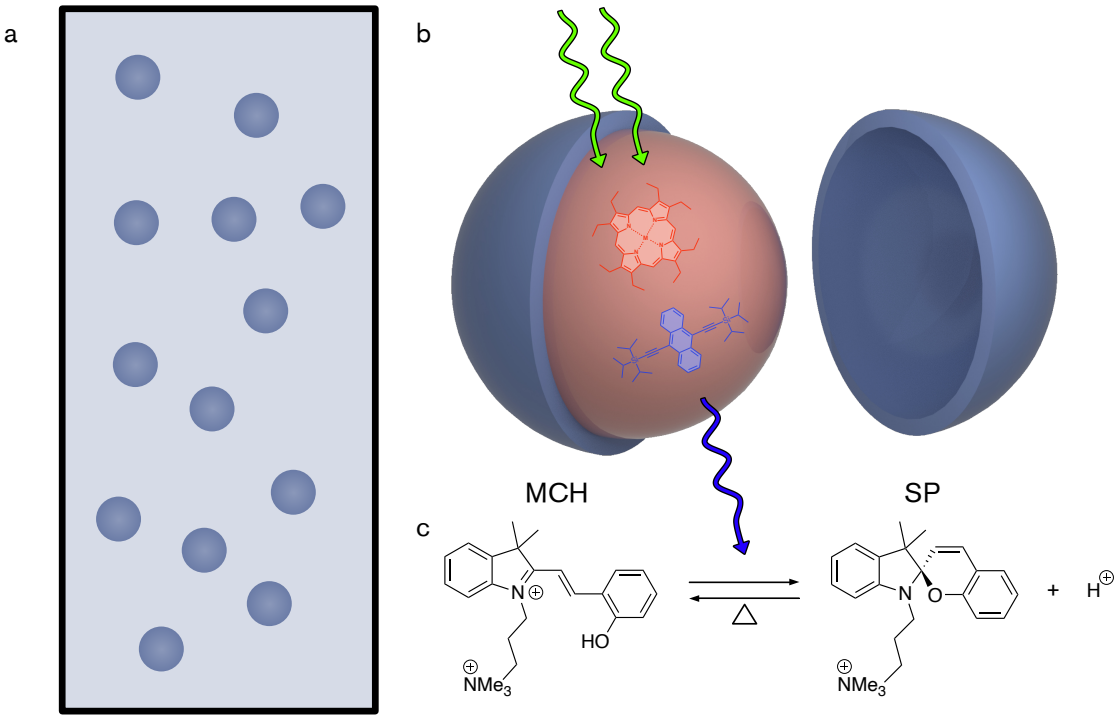

Figure 6.7: Overview of the TTA-UC-enabled photoisomerization of a spiropyran/merocyanine photoswitch. (a) Illustration depicting the complete system comprising upconverting microcapsules dispersed in water. (b) Schematic representation of the core-shell microcapsule architecture featuring the molecular structures of the upconversion molecules, specifically ZnOEP/PtOEP (red) and TIPS-An (blue). (c) Isomerization scheme of the spiropyran/merocyanine molecular photoswitch (omitting all intermediate species). The upconverted blue light initiates the MCH → SP isomerization process, subsequently triggering a deprotonation reaction, leading to both spectral alterations and a decrease in pH. The reverse isomerization reaction is thermally driven.

To confirm the formation of the microcapsules, aliquots of the prepared samples were imaged using fluorescence microscopy. Bright-field microscopy (Figure 6.8c) revealed microcapsules ranging in size from approximately 1 to 10 µm, with larger capsules displaying a discernible core, slightly brighter than the surrounding shell. Some capsules appeared collapsed, rendering them less prominent in the fluorescence images (Figure 6.8a,b). Excitation with 545 nm light revealed ZnOEP fluorescence, detectable with a red emission filter centered at 605 nm. ZnOEP, despite being a less efficient sensitizer than PtOEP, was chosen for these microscopy studies due to its fluorescent nature, facilitating easy monitoring under ambient conditions compared to the phosphorescent PtOEP. Figure 6.8a demonstrates stronger fluorescence intensity in the cores than in the shells, indicating predominant ZnOEP core localization. Conversely, PtOEP exhibited minimal emission (see the Supporting Information of **Paper IV**). Directly excited TIPS-An fluores-

cence was also notably stronger in the cores (Figure 6.8b; λ_{ex} = 365 nm, λ_{em} = 445 nm). Additionally, confocal microscopy was employed to image fluorescence from directly excited chromophores (Figure 2d, e).

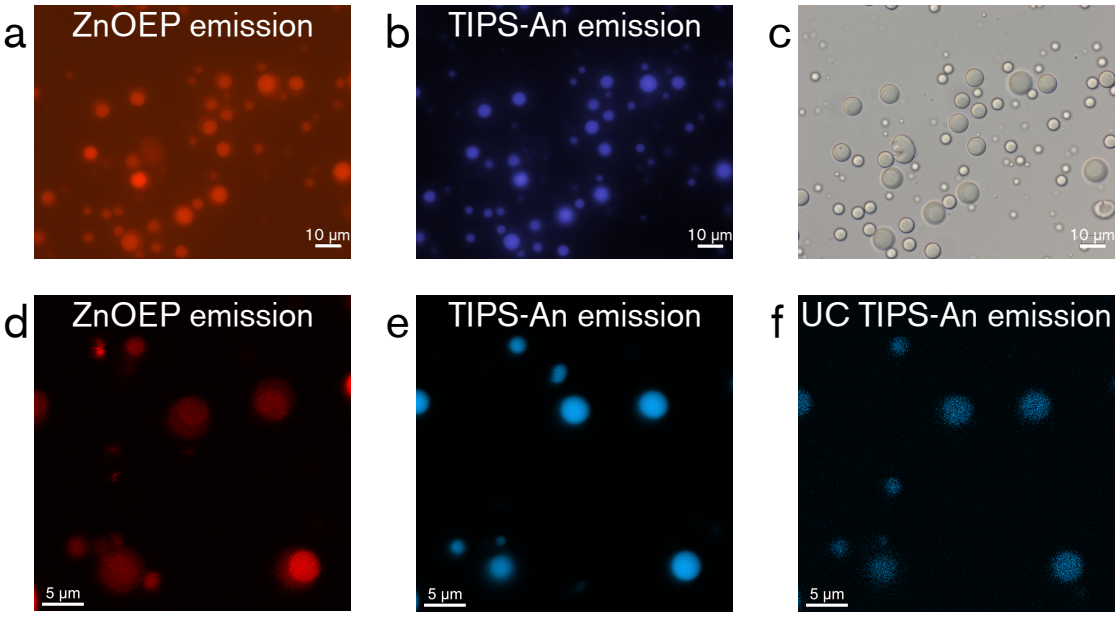

Figure 6.8: Microscopy images depict upconverting microcapsules (500 µM ZnOEP, 5 mM TIPS-An). (a)-(c) show the same area of the sample. (a) ZnOEP emission under fluorescence microscopy (λ_{ex} = 545/25 nm, λ_{em} = 605/70 nm). (b) TIPS-An emission under fluorescence microscopy (λ_{ex} = 365 nm, λ_{em} = 445/50 nm). (c) Brightfield microscopy revealing core-shell microcapsules. (d)-(f) show the same area of the sample. (d) Confocal microscopy displaying ZnOEP emission (λ_{ex} = 565 nm, λ_{em} = 580-700 nm). (e) Confocal microscopy exhibiting TIPS-An emission (λ_{ex} = 414 nm, λ_{em} = 430-500 nm). (f) Confocal microscopy showcasing upconverted TIPS-An emission (λ_{ex} = 565 nm, λ_{em} = 430-500 nm). Note that DMTM was included in the microcapsule core solution as a singlet oxygen scavenger to facilitate capture of the upconverted emission.

TTA-UC, reliant on long-lived triplet states, is, as previously stated, susceptible to oxygen quenching. Ideally, microcapsules would feature an oxygen impermeable shell, enabling an oxygen-free core at ambient conditions. However, our PLGA shell did not fully meet this criterion, necessitating oxygen removal from microcapsule samples for upconversion observation. The singlet oxygen scavenger dimethyl thiomethane (DMTM)[132] was introduced to the core solution to facilitate upconverted anti-Stokes emission detection in confocal microscopy (Figure 6.8f). Validation of the upconverted emission was achieved by imaging ZnOEP-only microcapsule samples under the same excitation conditions, yielding no emission signal (see the Supporting Information of **Paper IV**). Subsequent spectroscopic characterization involved oxygen removal via four freeze-pump-thaw cycles.

6.2.1 Comparing the TTA-UC Performance in Solution vs Microcapsules

Central to this study is the mitigation of the secondary inner-filter effect, which proved to be one of the major loss channels in **Paper III**, while preserving a high local TTA-UC chromophore concentration within the microcapsules. Re-absorption of upconverted light, primarily stemming from TIPS-An absorption and emission overlap, chiefly affects the highest energy TIPS-An emission peak in high concentration bulk solution TTA-UC samples. Figure 6.9 illustrates steady-state absorbance and upconverted emission comparisons between microcapsule and bulk solution samples. Microcapsules, formulated in water with a concentration of approximately 1.3 wt%, were diluted with 70% glycerol to minimize light scattering, resulting in negligible TTA-UC chromophore absorbance. Conversely, the bulk solution sample absorbance exceeded the measurable limit of the spectrophotometer (Abs $>$ 3).

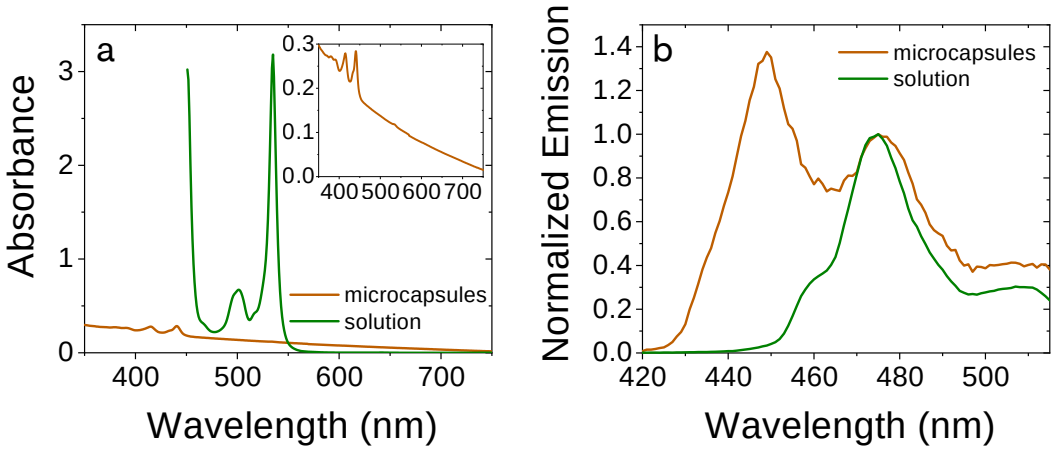

Figure 6.9: Steady-state absorption (a) and emission (λ_{ex} = 532 nm, 20.0 mW) (b) spectra of 50 µM PtOEP and 2 mM TIPS-An upconversion solutions in PLGA/glyceryl trioctanoate microcapsules (brown) and in a glyceryl trioctanoate solution (green). The inset in (a) provides a magnified view of the absorbance spectrum for the microcapsule sample. Both samples were measured in 10 mm x 10 mm cuvettes.

Moreover, Figure 6.9b demonstrates that the most blue-shifted band of upconverted TIPS-An fluorescence experiences greater attenuation in bulk solution samples compared to microcapsule counterparts. Experimental adjustments to minimize the secondary inner-filter effect were implemented for both sample types, with irradiation near the detector-facing cuvette wall in a right-angle measurement setup. The observed reduction in re-absorbed upconverted photons, particularly the high-energy fraction, underscores the potential of microcapsule-mediated upconversion for driving photochemical transformations requiring high energy light.

To ensure accurate characterization of the TTA-UC system's performance, time-resolved measurements were conducted on the micro-to-millisecond timescale, since the decay profiles of the sensitizer and annihilator emission are unaffected by light scattering. The samples comprised 50 µM PtOEP and 2.0 mM TIPS-An in a 1.3 wt% microcapsule solution in water, and a bulk solution sample with glyceryl trioctanoate as the solvent with the same chromophore concentration. Figure 6.10 illustrates the decay of upconverted emission in both microcapsule and solution samples, measured over a range of excitation intensities. Parameters such as the threshold excitation intensity (I_{th}) and the annihilator triplet lifetime (τ_T) were determined using the fitting procedure detailed in Equation (3.5). I_{th} for the bulk solution, determined for $\beta = 0.5$, was found to be 2.4 W cm^{-2}, compared to 227 mW cm^{-2} in the microcapsule sample. Looking at Figure 6.10a, it is clear to see that the decay of the upconverted emission could not be recorded at low enough excitation intensities to reach a non-annihilating annihilator triplet decay (i.e. a β approaching 0). This is thought to in part be due to the very low total chromophore concentration in the solution, giving rise to very low emission signals at low excitation intensities. Another factor is the high level of light scattering in the solution, which leads to a diminished intensity of the excitation light source throughout the sample. This means that the effective excitation intensity reaching the chromophores at the detection point mid-sample will not be as high as the measured excitation intensity. With this in mind, the I_{th} of the microcapsule sample might very well be much lower than what was estimated in this measurement.

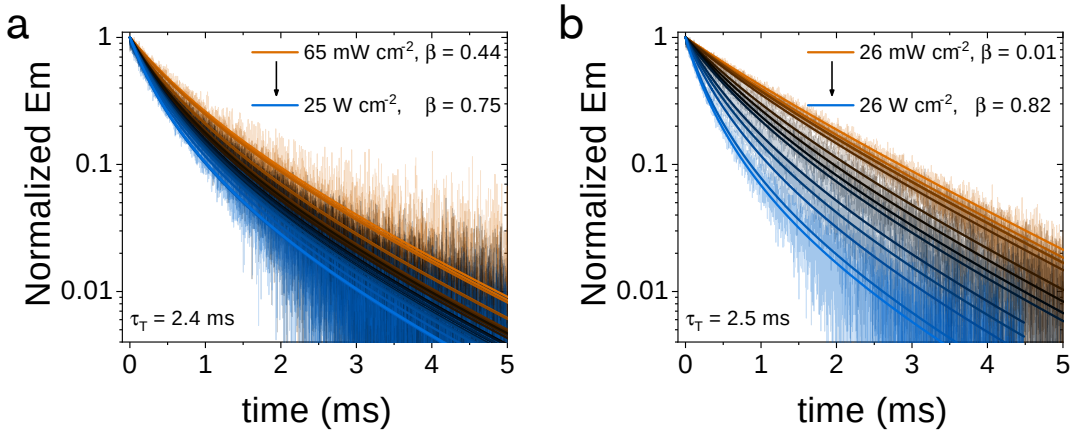

Figure 6.10: Time-resolved upconverted emission of 50 µM PtOEP and 2.0 mM TIPS-An in (a) microcapsules and (b) a glyceryl trioctanoate solution. Emission was measured at 451 nm (a) and 475 nm (b) upon 532 nm pulsed excitation at various intensities (as indicated in the figures). The fitting lines represent the best global fits of Equation (3.5), employing a shared τ_T.

Figure 6.11 illustrates the effective quenching of PtOEP phosphorescence by increasing the concentration of TIPS-An, both in the microcapsules and bulk solution, using a fixed PtOEP concentration of 50 µM. The Stern-Volmer equation (see Equation (3.3), was utilized to determine the triplet energy transfer rate (k_{TET}) from PtOEP to TIPS-An, representing the quenching pathway. The comparable k_{TET} values in microcapsules ($1.3 \cdot 10^8$ $M^{-1}s^{-1}$) and bulk solution ($1.1 \cdot 10^8$ $M^{-1}s^{-1}$) are similar to the diffusion rate constant at room temperature (estimated using the high viscosity of glyceryl trioctanoate[133]), suggesting a similar diffusion-controlled TET in both environments. Notably, while a monoexponential fit sufficed for the bulk solution, a biexponential fit was required for microcapsules with TIPS-An, indicating a long-lived decay component comparable to the non-quenched PtOEP lifetime. A very weak PtOEP phosphorescence in the microcapsule shell under ambient conditions suggests PtOEP localization in the PLGA shell instead of glyceryl trioctanoate cores, potentially explaining the observed long-lived PtOEP component. Additional details on fitting procedures are provided in the Supporting Information of **Paper IV**.

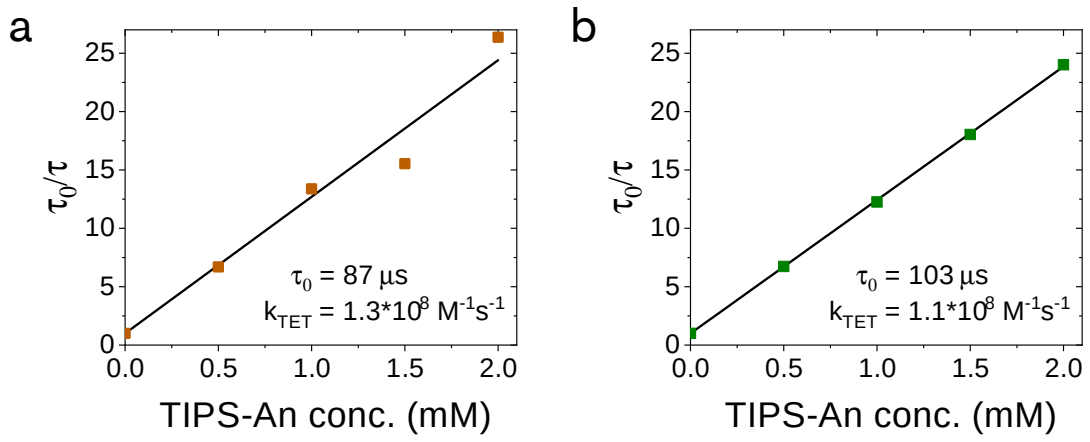

Figure 6.11: Stern-Volmer plots illustrating TET from 50 µM PtOEP to TIPS-An in (a) microcapsules and (b) a glyceryl trioctanoate solution, under excitation with a 532 nm laser at 260 mW cm^{-2} intensity.

6.2.2 TTA-UC Enhanced Isomerization and Deptrotonation of an SP/MC Photoswitch

To demonstrate the utilization of upconverted light from microcapsules in enabling a photochemical reaction, we employed the previously mentioned spiropyran/merocyanine photoacid. The goal was to trigger a deprotonation/isomerization reaction from the MCH form to the SP form using 532 nm light, chosen for its minimal direct isomerization potential due to the absorption properties of MCH. Samples were maintained at 5°C to disfavor the thermally induced back-reaction from SP

to MCH. Figure 6.12 illustrates the resulting absorption spectra of the photoisomerization under 532 nm light irradiation. The brown solid traces represent the equilibrated absorbance pre-irradiation, while the solid green trace with an overlaying dashed purple trace depicts the absorbance at the PSS. Even before degassing the sample, some isomerization occurred, indicating direct 532 nm-enabled isomerization from MCH to SP. After degassing to remove TTA-UC quenching oxygen, a higher degree of isomerization was observed, evident in the PSS. This difference is further highlighted in Figure 6.12, where the subtracted absorbance at PSS from the starting absorbance reveals the level of MCH to SP isomerization. Additionally, a differential absorption spectrum under 445 nm direct irradiation is included for comparison, showing that both 532 nm and 445 nm irradiation induce the sought after photoisomerization reaction, with the former amplified by upconverting microcapsules.

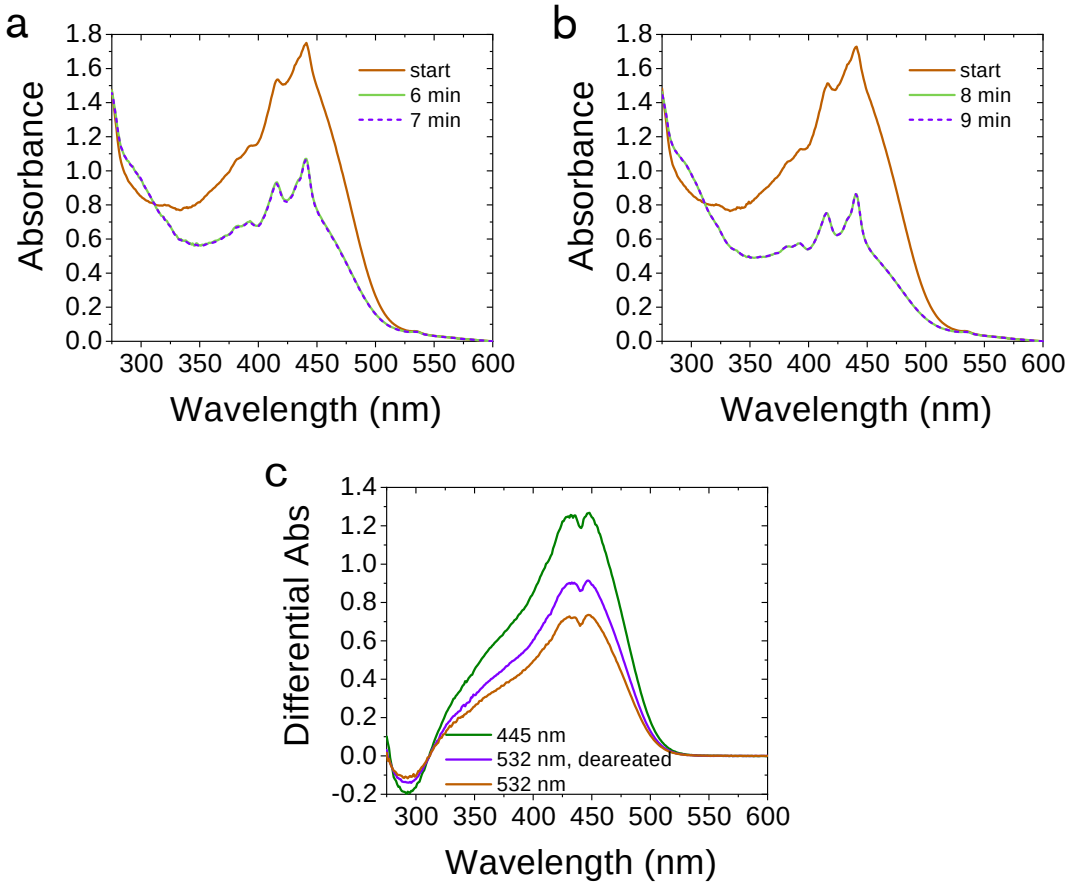

Figure 6.12: Absorption spectra depicting 532 nm-induced MCH → SP isomerization in a 2.4 wt% microcapsule sample with 50 µM PtOEP and 2.0 mM TIPS-An at an initial pH of 2.34 in a 30:70 water:glycerol solution. Panels (a) and (b) show absorbance before and after irradiation, with (b) representing a degassed sample. Panel (c) displays differential absorbance spectra for 445 nm and 532 nm irradiation on oxygen-containing and degassed samples.

By encapsulating TTA-UC molecules within water-dispersed microcapsules, the re-absorption losses from using bulk solutions in **Paper III** could be diminished. Through thorough spectroscopic and microscopic analysis, the efficacy of these microcapsules in facilitating TTA-UC-enabled reactions was validated. Time-resolved measurements unveil the dynamics of the upconversion process, while steady-state absorption measurements demonstrate the improved performance of photoisomerization and deprotonation reactions using the microcapsule system. Despite not achieving all intended goals, such as achieving oxygen impermeability, the findings offer valuable insights into optimizing encapsulated TTA-UC chromophores for driving photochemical reactions, particularly in aqueous environments.

7

Concluding Remarks and Outlook

The objective of this thesis is to use low energy light to control high energy photochemistry, as a means to overcome spectral mismatches between the available light and the light needed to control a photochemical process. Nature has been great at finding workarounds to this objective, but with the emergence of new technology in fields like solar energy conversion and life science, the need to modulate and manipulate light has emerged as an important tool. Molecular photoswitches from the DAE and SP families serve as model compounds for the high energy photochemistry in all four papers that this thesis is based on. Whilst serving as examples on high energy photochemistry, some of the studies have also shown that the modulated photochromic systems themselves could be used in future applications.

Chapter 4 shows how the fluorescence of a water-soluble DAE derivative (Dasy) could be rapidly modulated by light absorbed by the non-fluorescent isomer. The modulation frequencies strongly exceeded previous reports (250 Hz versus <1 Hz), and by using OLID this rapid modulation could also be distinguished from a bright background. In **Paper I** which this chapter is based on, this was also shown to work in a cellular environment. These results together with the other favorable properties of Dasy that are outlined in the study, show that Dasy is an excellent candidate for enhancing the contrast in OLID fluorescence imaging. A natural next step based on this study, would be to combine OLID with a fluorescence microscope to see the anticipated increased contrast.

The following two result chapters, namely Chapters 5 and 6, revolve around the common theme of using chemical methods to convert low energy light so that it can be used to control high energy photochemistry. Starting with Chapter 5, the findings presented herein show the versatility of using NC/molecular hybrid triplet sensitizers to achieve all-visible-light switching of DAE derivatives. The absorption bands of NCs can be easily tuned to match wavelength requirements of different photochemical reactions. In this study (further detailed in **Paper II**), the light

absorbed by the NC/molecular hybrids does not have enough energy to directly drive the DAE photoisomerization reactions through singlet excitation. Instead, the reaction is driven using the lower lying triplet manifold of the DAEs with the NC/molecular hybrids acting as triplet sensitizers. This approach improved the fatigue resistance of the DAEs, while maintaining comparable isomerization quantum yields to using UV light. Further steps towards bio-applicability could involve using two-photon absorption to gain deeper tissue penetration, coating the CdS NCs with nontoxic organic molecules or polymers, or functionalizing DAE derivatives with carboxylic acid functional groups to remove the need of mediators.

Chapter 6 covers the research in **Paper III** and **Paper IV**, in which low energy light is upconverted to high energy light through the process of TTA-UC. Since the high energy needed to enable the photochemical reactions is now carried by photons instead of molecules or particles, such as in triplet sensitization, the light manipulating species and the photoreactant no longer have to be in molecular contact for the reaction to proceed. The first part of the chapter focuses on a project in which TTA-UC enabled single wavelength control of both reversible photoisomerization and fluorescence of DAEs. While the setup was proven both simple and versatile, the TTA-UC-driven photoisomerization was not very efficient as compared to direct UV isomerization. One of the loss factors found in this study was that of inherent re-absorption of the upconverted light. This was one of the aims to improve upon in the second part of the chapter, in which the TTA-UC system is confined into core-shell microcapsules. The encapsulation allowed for driving photochemistry in water, which was exemplified by boosting the photoisomerization of an SP/MC photoacid. Although both studies have proven to have their own inherent problems, they can hopefully serve as a source of knowledge for future use of TTA-UC to drive photochemical reactions.

In summary, this thesis has demonstrated significant advances in the utilization of low-energy light to govern high-energy photochemistry, addressing the challenge of spectral mismatches in controlling photochemical processes. Through the exploration of various molecular systems, this work has elucidated strategies to modulate and manipulate light effectively for targeted applications. From achieving rapid modulation of fluorescence in cellular environments to enabling all-visible-light switching of photochemical reactions, the findings presented here pave the way for enhanced contrast imaging and biocompatible photochemistry. Furthermore, the investigations involving TTA-UC offer promising avenues for single-wavelength control and water-compatible photochemistry. Moving forward, further optimization and mechanistic understanding will be crucial to realizing the full potential of visible-light control in high-energy photochemical transformations.

8

Acknowledgements

This roller coaster of a ride that pursuing a PhD has been, would not have been half as enjoyable without the help and support from the people around me. Thank you all for that! I especially would like to mention some of you.

First of all, I want to thank my supervisor Bo Albinsson. Five years ago, when I applied for a PhD position in your group, you told me that you wanted your research to be a learning tool for your students, rather than your students being a tool for you to produce papers. You have throughout these years stayed true to these words, which has helped pushing me to take on new challenges without being hindered by the fear of failure. Your curiosity and enthusiasm for science and teaching is truly inspiring, and I am very grateful for your guidance and support throughout these years. I also want to thank my co-supervisor Joakim Andréasson for being very involved in all of my research projects, and always taking your time to sit down and help me understand things that I have not been able to wrap my head around on my own. The two of you make the best supervisory team I could ever have asked for, and I am thankful for both the scientific discussions and the laughs!

I am grateful for the support from Jerker Mårtensson who has followed my learning journey both as my examiner and line manager. Thank you Anna Molander, Gunilla Saethe, Lynga Huang Normann, Marcus Wilhelmsson, Nina Kann and Sara da Costa for always helping out with various matters throughout my employment at Chalmers, big or small. Björn Åkerman, Nikola Marcovic and Per Lincoln - you have been great role models for me, starting as teachers during my early Chalmers years and even more during my PhD studies as three of my friendliest colleagues.

A special mention also goes out to Maria Abrahamsson, for guidance both as a scientist and dear colleague. The weekly spectroscopy group meetings that you have organized throughout these years have been a great source of knowledge and inspiration, and it has for sure helped bringing us PhD students and postdocs closer

together. For this, I of course also want to thank past and present members of this group: Rasmus, Fredrik, Elin, Andrew, Axel, Carlos, Liam, Jean, Deise, Long, Gerard, Letizia, Jessica, Hanna, Hassan, Pauline, Alma, Andrea, Lili, Gaowa, Björn and Cassandra. The great discussions both regarding our own research and during our Journal Club meetings have taught me a lot. That, together with your support both in the lab and as compassionate people have really brightened many of my days. Thank you also to Hanna, Hassan, Jesper, Lili and Pauline for proofreading parts of the thesis, and to Gaowa, Lili, Fredrik, Axel, Wilma, Viktor and Jessica for our time in the lab working on shared projects.

Working on floor five comes with a great work environment - thank you all for the great lunch room chats, friendly faces in the corridors and nice after works!

A heartfelt thank you goes out to my past and present office mates in 5064. Thank you Jesper and Fredrik for making me feel welcome from my very first day, and thank you Pauline and Hanna for keeping up the wonderful spirit of our office during my last year at Chalmers. I consider you all dear friends.

Finally, I would like to thank all my friends and family for reminding me that life consists of so many more beautiful things than work. My dear parents Tarja and Jörgen, together with my sister Tove, for your endless love and support. My life partner David, with you and our furry companion Zia I get to live my dream life.

Wera Larsson, Gothenburg, March 2024

Bibliography

[1] M. P. Johnson. Photosynthesis. *Essays in Biochemistry* **2016**, *60*(*3*), 255–273.

[2] N. S. Lewis and D. G. Nocera. Powering the planet: Chemical challenges in solar energy utilization. *Proceedings of the National Academy of Sciences* **2006**, *103*(*43*), 15729–15735.

[3] L. C. Andreani, A. Bozzola, P. Kowalczewski, M. Liscidini, and L. Redorici. Silicon solar cells: toward the efficiency limits. *Advances in Physics: X* **2019**, *4*(*1*).

[4] W. Bludau, A. Onton, and W. Heinke. Temperature dependence of the band gap of silicon. *Journal of Applied Physics* **1974**, *45*(*4*), 1846–1848.

[5] W. Shockley and H. J. Queisser. Detailed Balance Limit of Efficiency of p-n Junction Solar Cells. *Journal of Applied Physics* **1961**, *32*(*3*), 510–519.

[6] A. Fujishima and K. Honda. Electrochemical Photolysis of Water at a Semiconductor Electrode. *Nature* **1972**, *238*, 37–38.

[7] A. J. Bard and M. A. Fox. Artificial Photosynthesis: Solar Splitting of Water to Hydrogen and Oxygen. *Accounts of Chemical Research* **1995**, *28*(*3*), 141–145.

[8] W. A. Velema, W. Szymanski, and B. L. Feringa. Photopharmacology: beyond proof of principle. *Journal of the American Chemical Society* **2014**, *136*(*6*), 2178–2191.

[9] J. Broichhagen, J. A. Frank, and D. Trauner. A roadmap to success in photopharmacology. *Account of Chemical Research* **2015**, *48*(*7*), 1947–1960.

[10] T. J. Dougherty, C. J. Gomer, B. W. Henderson, G. Jori, D. Kessel, M. Ko-

rbelik, J. Moan, and Q. Peng. Photodynamic therapy. *JNCI: Journal of the National Cancer Institute* **1998**, *90*(*12*), 889–905.

[11] M. Monici. *Biotechnology Annual Review: Cell and tissue autofluorescence research and diagnostic applications*, volume 11, pages 227–256. Elsevier, 2005.

[12] M. B. Smith and J. Michl. Singlet fission. *Chemical Reviews* **2010**, *110*(*11*), 6891–6936.

[13] IUPAC. *photochromism*. International Union of Pure and Applied Chemistry (IUPAC), 3.0.1 edition, 2019.

[14] B. L. Feringa and W. R. Browne, editors. *Molecular Switches*. Wiley-VCH Verlag & Co., Weinheim, Germany, 2nd edition, 2011.

[15] G. S. Hammond, N. J. Turro, and P. A. Leermakers. The mechanisms of photoreactions in solution. IX. Energy transfer from the triplet states of aldehydes and ketones to unsaturated compounds[1]. *The Journal of Physical Chemistry* **1962**, *66*(*6*), 1144–1147.

[16] L. D. Elliott, S. Kayal, M. W. George, and K. Booker-Milburn. Rational design of triplet sensitizers for the transfer of excited state photochemistry from uv to visible. *Journal of the American Chemical Society* **2020**, *142*(*35*), 14947–14956.

[17] L. Hou, W. Larsson, S. Hecht, J. Andréasson, and B. Albinsson. A general approach for all-visible-light switching of diarylethenes through triplet sensitization using semiconducting nanocrystals. *Journal of Materials Chemistry C* **2022**, *10*(*42*), 15833–15842.

[18] M. Pawlicki, H. A. Collins, R. G. Denning, and H. L. Anderson. Two-photon absorption and the design of two-photon dyes. *Angewandte Chemie International Edition* **2009**, *48*(*18*), 3244–3266.

[19] P. A. Franken, A. E. Hill, C. W. Peters, and G. Weinreich. Generation of optical harmonics. *Physical Review Letters* **1961**, *7*(*4*), 118–119.

[20] M. Haase and H. Schäfer. Upconverting nanoparticles. *Angewandte Chemie International Edition* **2011**, *50*(*26*), 5808–5829.

[21] C. A. Parker, C. G. Hatchard, and E. J. Bowen. Delayed fluorescence from solutions of anthracene and phenanthrene. *Proceedings of the Royal Society*

of London. Series A. Mathematical and Physical Sciences **1962**, *269*(*1339*), 574–584.

[22] T. N. Singh-Rachford and F. N. Castellano. Photon upconversion based on sensitized triplet–triplet annihilation. *Coordination Chemistry Reviews* **2010**, *254*(*21-22*), 2560–2573.

[23] J. Feng, J. Alves, D. M. de Clercq, and T. W. Schmidt. Photochemical upconversion. *Annual Review of Physical Chemistry* **2023**, *74*(*1*), 145–168.

[24] S. Baluschev, T. Miteva, V. Yakutkin, G. Nelles, A. Yasuda, and G. Wegner. Up-conversion fluorescence: Noncoherent excitation by sunlight. *Physical Review Letters* **2006**, *97*(*14*), 143903.

[25] R. R. Islangulov, J. Lott, C. Weder, and F. N. Castellano. Noncoherent low-power upconversion in solid polymer films. *Journal of the American Chemical Society* **2007**, *129*(*42*), 12652–12653.

[26] A. Haefele, J. Blumhoff, R. S. Khnayzer, and F. N. Castellano. Getting to the (square) root of the problem: How to make noncoherent pumped upconversion linear. *The Journal of Physical Chemistry Letters* **2012**, *3*(*3*), 299–303.

[27] J. M. Hollas. *Modern Spectroscopy*. John Wiley & Sons, Chichester, England, fourth edition, 2004.

[28] P. Atkins, J. de Paula, and R. Friedman. *Physical chemistry: quanta, matter, and change*. Oxford University Press, Oxford, United Kingdom, second edition edition, 2014.

[29] C. Grewer and H.-D. Brauer. Mechanism of the triplet-state quenching by molecular oxygen in solution. *The Journal of Physical Chemistry* **1994**, *98*(*16*), 4230–4235.

[30] T. Förster. Zwischenmolekulare energiewanderung und fluoreszenz. *Annalen der Physik* **1948**, *437*(*1-2*), 55–75.

[31] D. L. Dexter. A theory of sensitized luminescence in solids. *The Journal of Chemical Physics* **1953**, *21*(*5*), 836–850.

[32] M. Irie. Diarylethenes for memories and switches. *Chemical Reviews* **2000**, *100*(*5*), 1685–1716.

[33] M. Irie, T. Fukaminato, K. Matsuda, and S. Kobatake. Photochromism of diarylethene molecules and crystals: Memories, switches, and actuators. *Chemical Reviews* **2014**, *114*(*24*), 12174–12277.

[34] M. Irie. *Diarylethene Molecular Photoswitches: Concepts and Functionalities*. Wiley-VCH GmbH, Weinheim, Germany, 1 edition, 2021.

[35] T. Leydecker, M. Herder, E. Pavlica, G. Bratina, S. Hecht, E. Orgiu, and P. Samori. Flexible non-volatile optical memory thin-film transistor device with over 256 distinct levels based on an organic bicomponent blend. *Nature Nanotechnology* **2016**, *11*(*9*), 769–775.

[36] L. Hou, X. Zhang, G. F. Cotella, G. Carnicella, M. Herder, B. M. Schmidt, M. Pätzel, S. Hecht, F. Cacialli, and P. Samorì. Optically switchable organic light-emitting transistors. *Nature Nanotechnology* **2019**, *14*(*4*), 347–353.

[37] Y. Zou, T. Yi, S. Xiao, F. Li, C. Li, X. Gao, J. Wu, M. Yu, and C. Huang. Amphiphilic Diarylethene as a Photoswitchable Probe for Imaging Living Cells. *Journal of the American Chemical Society* **2008**, *130*(*47*), 15750–15751.

[38] K. Uno, M. L. Bossi, V. N. Belov, M. Irie, and S. W. Hell. Multicolour fluorescent "sulfide-sulfone" diarylethenes with high photo-fatigue resistance. *Chemical Communications* **2020**, *56*(*14*), 2198–2201.

[39] E. Fischer and Y. Hirshberg. Formation of coloured forms of spirans by low-temperature irradiation. *Journal of the Chemical Society* **1952**, pages 4522–4524.

[40] C. J. Martin, G. Rapenne, T. Nakashima, and T. Kawai. Recent progress in development of photoacid generators. *Journal of Photochemistry and Photobiology C: Photochemistry Reviews* **2018**, *34*, 41–51.

[41] L. Wimberger, S. K. K. Prasad, M. D. Peeks, J. Andréasson, T. W. Schmidt, and J. E. Beves. Large, tunable, and reversible ph changes by merocyanine photoacids. *Journal of the American Chemical Society* **2021**, *143*(*49*), 20758–20768.

[42] A. Nayak, H. Liu, and G. Belfort. An optically reversible switching membrane surface. *Angewandte Chemie International Edition* **2006**, *45*(*25*), 4094–4098.

[43] Y. Hirshberg. Reversible formation and eradication of colors by irradiation at low temperatures. a photochemical memory model. *Journal of the American Chemical Society* **1956**, *78*(*10*), 2304–2312.

[44] C. J. F. Rijcken, O. Soga, W. E. Hennink, and C. F. van Nostrum. Triggered destabilisation of polymeric micelles and vesicles by changing polymers polarity: an attractive tool for drug delivery. *Journal of Controlled Release* **2007**, *120*(*3*), 131–148.

[45] R. T. F. Jukes, V. Adamo, F. Hartl, P. Belser, and L. De Cola. Photochromic Dithienylethene Derivatives Containing Ru(II) or Os(II) Metal Units. Sensitized Photocyclization from a Triplet State. *Inorganic Chemistry* **2004**, *43*(*9*), 2779–2792.

[46] V. W.-W. Yam, C.-C. Ko, and N. Zhu. Photochromic and Luminescence Switching Properties of a Versatile Diarylethene-Containing 1,10-Phenanthroline Ligand and Its Rhenium(I) Complex. *Journal of the American Chemical Society* **2004**, *126*(*40*), 12734–12735.

[47] S. Fredrich, R. Göstl, M. Herder, L. Grubert, and S. Hecht. Switching Diarylethenes Reliably in Both Directions with Visible Light. *Angewandte Chemie International Edition* **2016**, *55*(*3*), 1208–1212.

[48] Z. Zhang, W. Wang, P. Jin, J. Xue, L. Sun, J. Huang, J. Zhang, and H. Tian. A building-block design for enhanced visible-light switching of diarylethenes. *Nature Communications* **2019**, *10*(*1*), 4232.

[49] Z. Zhang, J. Zhang, B. Wu, X. Li, Y. Chen, J. Huang, L. Zhu, and H. Tian. Diarylethenes with a narrow singlet–triplet energy gap sensitizer: a simple strategy for efficient visible-light photochromism. *Advanced Optical Materials* **2018**, *6*(*6*), 1700847.

[50] C. Grewer and H.-D. Brauer. Mechanism of the Triplet-State Quenching by Molecular Oxygen in Solution. *Journal of Physical Chemistry* **1994**, *98*(*16*), 4230–4235.

[51] C. G. Hübner, A. Renn, I. Renge, and U. P. Wild. Direct observation of the triplet lifetime quenching of single dye molecules by molecular oxygen. *The Journal of Chemical Physics* **2001**, *115*(*21*), 9619–9622.

[52] C. Schweitzer and R. Schmidt. Physical Mechanisms of Generation and Deactivation of Singlet Oxygen. *Chemical Reviews* **2003**, *103*(*5*), 1685–1758.

[53] Y. Zhou, F. N. Castellano, T. W. Schmidt, and K. Hanson. On the Quantum Yield of Photon Upconversion via Triplet–Triplet Annihilation. *ACS Energy Letters* **2020**, *5*(*7*), 2322–2326.

[54] W. Sun, A. Ronchi, T. Zhao, J. Han, A. Monguzzi, and P. Duan. Highly efficient photon upconversion based on triplet–triplet annihilation from bichromophoric annihilators. *Journal of Materials Chemistry C* **2021**, *9*(*40*), 14201–14208.

[55] A. Olesund, J. Johnsson, F. Edhborg, S. Ghasemi, K. Moth-Poulsen, and B. Albinsson. Approaching the Spin-Statistical Limit in Visible-to-Ultraviolet Photon Upconversion. *Journal of the American Chemical Society* **2022**, *144*(*8*), 3706–3716.

[56] T. Trupke, A. Shalav, B. S. Richards, P. Würfel, and M. A. Green. Efficiency enhancement of solar cells by luminescent up-conversion of sunlight. *Solar Energy Materials and Solar Cells* **2006**, *90*(*18-19*), 3327–3338.

[57] Y. Y. Cheng, A. Nattestad, T. F. Schulze, R. W. MacQueen, B. Fückel, K. Lips, G. G. Wallace, T. Khoury, M. J. Crossley, and T. W. Schmidt. Increased upconversion performance for thin film solar cells: a trimolecular composition. *Chemical Science* **2016**, *7*(*1*), 559–568.

[58] Y. L. Lin, M. Koch, A. N. Brigeman, D. M. E. Freeman, L. Zhao, H. Bronstein, N. C. Giebink, G. D. Scholes, and B. P. Rand. Enhanced subbandgap efficiency of a solid-state organic intermediate band solar cell using triplet–triplet annihilation. *Energy & Environmental Science* **2017**, *10*(*6*), 1465–1475.

[59] E. M. Gholizadeh, S. K. K. Prasad, Z. L. Teh, T. Ishwara, S. Norman, A. J. Petty, J. H. Cole, S. Cheong, R. D. Tilley, J. E. Anthony, S. Huang, and T. W. Schmidt. Photochemical upconversion of near-infrared light from below the silicon bandgap. *Nature Photonics* **2020**, *14*(*9*), 585–590.

[60] D. Beery, T. W. Schmidt, and K. Hanson. Harnessing sunlight via molecular photon upconversion. *ACS Applied Materials & Interfaces* **2021**, *13*(*28*), 32601–32605.

[61] R. S. Khnayzer, J. Blumhoff, J. A. Harrington, A. Haefele, F. Deng, and F. N. Castellano. Upconversion-powered photoelectrochemistry. *Chemical Communications* **2012**, *48*(*2*), 209–211.

[62] K. Börjesson, D. Dzebo, B. Albinsson, and K. Moth-Poulsen. Photon upconversion facilitated molecular solar energy storage. *Journal of Materials Chemistry A* **2013**, *1*(*30*), 8521–8524.

[63] C. Ye, J. Wang, X. Wang, P. Ding, Z. Liang, and X. Tao. A new medium for triplet–triplet annihilated upconversion and photocatalytic application. *Physical Chemistry Chemical Physics* **2016**, *18*(*5*), 3430–3437.

[64] S. Chandrasekaran, Y.-L. T. Ngo, L. Sui, E. J. Kim, D. K. Dang, J. S. Chung, and S. H. Hur. Highly enhanced visible light water splitting of CdS by green to blue upconversion. *Dalton Transactions* **2017**, *46*(*40*), 13912–13919.

[65] A. Monguzzi, A. Oertel, D. Braga, A. Riedinger, D. K. Kim, P. N. Knüsel, A. Bianchi, M. Mauri, R. Simonutti, D. J. Norris, and F. Meinardi. Photocatalytic water-splitting enhancement by sub-bandgap photon harvesting. *ACS Applied Materials & Interfaces* **2017**, *9*(*46*), 40180–40186.

[66] Y. Liu, T. Yu, Y. Zeng, J. Chen, G. Yang, and Y. Li. Coupling red-to-blue upconversion organic microcrystals with $Cd_{0.5}Zn_{0.5}S$ for efficient and durable photocatalytic hydrogen production. *Chemistry – An Asian Journal* **2022**, *17*(*13*), e202200343.

[67] O. S. Kwon, J.-H. Kim, J. K. Cho, and J.-H. Kim. Triplet–triplet annihilation upconversion in CdS-decorated SiO_2 nanocapsules for sub-bandgap photocatalysis. *ACS Applied Materials & Interfaces* **2015**, *7*(*1*), 318–325.

[68] D. C. Thévenaz, A. Monguzzi, D. Vanhecke, R. Vadrucci, F. Meinardi, Y. C. Simon, and C. Weder. Thermoresponsive low-power light upconverting polymer nanoparticles. *Materials Horizons* **2016**, *3*(*6*), 602–607.

[69] J.-H. Kang, S.-H. Kim, A. Fernandez-Nieves, and E. Reichmanis. Amplified photon upconversion by photonic shell of cholesteric liquid crystals. *Journal of the American Chemical Society* **2017**, *139*(*16*), 5708–5711.

[70] Q. Liu, M. Xu, T. Yang, B. Tian, X. Zhang, and F. Li. Highly Photostable Near-IR-Excitation Upconversion Nanocapsules Based on Triplet–Triplet Annihilation for in Vivo Bioimaging Application. *ACS Applied Materials & Interfaces* **2018**, *10*(*12*), 9883–9888.

[71] S. N. Sanders, M. K. Gangishetty, M. Y. Sfeir, and D. N. Congreve. Photon upconversion in aqueous nanodroplets. *Journal of the American Chemical Society* **2019**, *141*(*23*), 9180–9184.

[72] H. Lee, M.-S. Lee, M. Uji, N. Harada, J.-M. Park, J. Lee, S. E. Seo, C. S. Park, J. Kim, S. J. Park, S. H. Bhang, N. Yanai, N. Kimizuka, O. S. Kwon, and J.-H. Kim. Nanoencapsulated phase-change materials: Versatile and air-tolerant platforms for triplet–triplet annihilation upconversion. *ACS Applied Materials & Interfaces* **2022**, *14*(*3*), 4132–4143.

[73] R. Jeyaseelan, M. Utikal, C. G. Daniliuc, and L. Næsborg. Photocyclization by a triplet–triplet annihilation upconversion pair in water – avoiding UV-light and oxygen removal. *Chemical Science* **2023**, *14*(*40*), 11040–11044.

[74] B. Zhang, K. D. Richards, B. E. Jones, A. R. Collins, R. Sanders, S. R. Needham, P. Qian, A. Mahadevegowda, C. Ducati, S. W. Botchway, and R. C. Evans. Ultra-small air-stable triplet-triplet annihilation upconversion nanoparticles for anti-stokes time-resolved imaging. *Angewandte Chemie International Edition* **2023**, *62*(*47*), e202308602.

[75] A. Loxley and B. Vincent. Preparation of poly(methylmethacrylate) microcapsules with liquid cores. *Journal of Colloid and Interface Science* **1998**, *208*(*1*), 49–62.

[76] V. Eriksson, L. Beckerman, E. Aerts, M. Andersson Trojer, and L. Evenäs. Polyanhydride microcapsules exhibiting a sharp pH transition at physiological conditions for instantaneous triggered release. *Langmuir* **2023**, *39*(*49*), 18003–18010.

[77] J. R. Lakowicz. *Principles of Fluorescence Spectroscopy*. Springer, Baltimore, Maryland, USA, third edition, 2006.

[78] F. Edhborg, A. Olesund, and B. Albinsson. Best practice in determining key photophysical parameters in triplet-triplet annihilation photon upconversion. *Photochemical & Photobiological Sciences* **2022**, *21*(*7*), 1143–1158.

[79] A. Monguzzi, J. Mezyk, F. Scotognella, R. Tubino, and F. Meinardi. Upconversion-induced fluorescence in multicomponent systems: Steady-state excitation power threshold. *Physical Review B* **2008**, *78*(*19*), 195112.

[80] U. Kubitscheck, editor. *Fluorescence Microscopy: From Principles to Biological Applications*. Wiley-VCH Verlag GmbH & Co, Weinheim, Germany, 2017.

[81] G. Naren, W. Larsson, C. Benitez-Martin, S. Li, E. Pérez-Inestrosa, B. Albinsson, and J. Andréasson. Rapid amplitude-modulation of a diarylethene

photoswitch: en route to contrast-enhanced fluorescence imaging. *Chemical Science* **2021**, *12*(*20*), 7073–7078.

[82] G. Naren, S. Li, and J. Andréasson. A simplicity-guided cocktail approach toward multicolor fluorescent systems. *Chemical Communications* **2020**, *56*(*23*), 3377–3380.

[83] K. Shibata, L. Kuroki, T. Fukaminato, and M. Irie. Fluorescence Switching of a Diarylethene Derivative Having Oxazole Rings. *Chemistry Letters* **2008**, *37*(*8*), 832–833.

[84] A. E. Keirstead, J. W. Bridgewater, Y. Terazono, G. Kodis, S. D. Straight, P. A. Liddell, A. L. Moore, T. A. Moore, and D. Gust. Photochemical "Triode" Molecular Signal Transducer. *Journal of the American Chemical Society* **2010**, *132*(*18*), 6588–6595.

[85] G. Copley, J. G. Gillmore, J. Crisman, G. Kodis, C. L. Gray, B. R. Cherry, B. D. Sherman, P. A. Liddell, M. M. Paquette, L. Kelbauskas, N. L. Frank, A. L. Moore, T. A. Moore, and D. Gust. Modulating Short Wavelength Fluorescence with Long Wavelength Light. *Journal of the American Chemical Society* **2014**, *136*(*34*), 11994–12003.

[86] S. Mao, R. K. Benninger, Y. Yan, C. Petchprayoon, D. Jackson, C. J. Easley, D. W. Piston, and G. Marriott. Optical Lock-In Detection of FRET Using Synthetic and Genetically Encoded Optical Switches. *Biophysical Journal* **2008**, *94*(*11*), 4515–4524.

[87] C. Petchprayoon, Y. Yan, S. Mao, and G. Marriott. Rational design, synthesis, and characterization of highly fluorescent optical switches for high-contrast optical lock-in detection (OLID) imaging microscopy in living cells. *Bioorganic & Medicinal Chemistry* **2011**, *19*(*3*), 1030–1040.

[88] Z. Tian, W. Wu, W. Wan, and A. D. Q. Li. Photoswitching-induced frequency-locked donor-acceptor fluorescence double modulations identify the target analyte in complex environments. *Journal of the American Chemical Society* **2011**, *133*(*40*), 16092–16100.

[89] Y. Yan, C. Petchprayoon, S. Mao, and G. Marriott. Reversible optical control of cyanine fluorescence in fixed and living cells: optical lock-in detection immunofluorescence imaging microscopy. *Philosophical Transactions of the Royal Society B: Biological Sciences* **2013**, *368*(*1611*), 20120031.

[90] G. Marriott, S. Mao, T. Sakata, J. Ran, D. K. Jackson, C. Petchprayoon, T. J. Gomez, E. Warp, O. Tulyathan, H. L. Aaron, E. Y. Isacoff, and Y. Yan. Optical lock-in detection imaging microscopy for contrast-enhanced imaging in living cells. *Proceedings of the National Academy of Sciences of the United States of America* **2008**, *105*(*46*), 17789–17794.

[91] L. Wu, Y. Dai, X. Jiang, C. Petchprayoon, J. E. Lee, T. Jiang, Y. Yan, and G. Marriott. High-contrast fluorescence imaging in fixed and living cells using optimized optical switches. *PLoS One* **2013**, *8*(*6*), e64738.

[92] J. R. Nilsson, S. Li, B. Önfelt, and J. Andréasson. Light-induced cytotoxicity of a photochromic spiropyran. *Chemical Communications* **2011**, *47*(*39*), 11020–11022.

[93] D. Bléger and S. Hecht. Visible-Light-Activated Molecular Switches. *Angewandte Chemie International Edition* **2015**, *54*(*39*), 11338–11349.

[94] Z. Zhang, W. Wang, M. O'Hagan, J. Dai, J. Zhang, and H. Tian. Stepping Out of the Blue: From Visible to Near-IR Triggered Photoswitches. *Angewandte Chemie International Edition* **2022**, *61*(*31*), e202205758.

[95] G. M. Tsivgoulis and J.-M. Lehn. Multiplexing optical systems: Multicolor-bifluorescent-biredox photochromic mixtures. *Advanced Materials* **1997**, *9*(*8*), 627–630.

[96] T. Fukaminato, T. Hirose, T. Doi, M. Hazama, K. Matsuda, and M. Irie. Molecular Design Strategy toward Diarylethenes That Photoswitch with Visible Light. *Journal of the American Chemical Society* **2014**, *136*(*49*), 17145–17154.

[97] J.-C. Boyer, C.-J. Carling, B. D. Gates, and N. R. Branda. Two-Way Photoswitching Using One Type of Near-Infrared Light, Upconverting Nanoparticles, and Changing Only the Light Intensity. *Journal of the American Chemical Society* **2010**, *132*(*44*), 15766–15772.

[98] T. Wu and N. R. Branda. Using low-energy near infrared light and upconverting nanoparticles to trigger photoreactions within supramolecular assemblies. *Chemical Communications* **2016**, *52*(*56*), 8636–8644.

[99] M. Irie, T. Lifka, K. Uchida, S. Kobatake, and Y. Shindo. Fatigue resistant properties of photochromic dithienylethenes: by-product formation. *Chemical Communications* **1999**, (*8*), 747–750.

[100] M. Herder, B. M. Schmidt, L. Grubert, M. Pätzel, J. Schwarz, and S. Hecht. Improving the Fatigue Resistance of Diarylethene Switches. *Journal of the American Chemical Society* **2015**, *137*(*7*), 2738–2747.

[101] X. Michalet, F. F. Pinaud, L. A. Bentolila, J. M. Tsay, S. Doose, J. J. Li, G. Sundaresan, A. M. Wu, S. S. Gambhir, and S. Weiss. Quantum Dots for Live Cells, in Vivo Imaging, and Diagnostics. *Science* **2005**, *307*(*5709*), 538–544.

[102] Q. Sun, Y. A. Wang, L. S. Li, D. Wang, T. Zhu, J. Xu, C. Yang, and Y. Li. Bright, multicoloured light-emitting diodes based on quantum dots. *Nature Photonics* **2007**, *1*(*12*), 717–722.

[103] X. Dai, Z. Zhang, Y. Jin, Y. Niu, H. Cao, X. Liang, L. Chen, J. Wang, and X. Peng. Solution-processed, high-performance light-emitting diodes based on quantum dots. *Nature* **2014**, *515*(*7525*), 96–99.

[104] A. P. Alivisatos. Semiconductor Clusters, Nanocrystals, and Quantum Dots. *Science* **1996**, *271*(*5251*), 933–937.

[105] R. Rossetti, S. Nakahara, and L. E. Brus. Quantum size effects in the redox potentials, resonance Raman spectra, and electronic spectra of CdS crystallites in aqueous solution. *The Journal of Chemical Physics* **1983**, *79*(*2*), 1086–1088.

[106] X. Wang, J. Zhuang, Q. Peng, and Y. Li. A general strategy for nanocrystal synthesis. *Nature* **2005**, *437*(*7055*), 121–124.

[107] N. J. Thompson, M. W. B. Wilson, D. N. Congreve, P. R. Brown, J. M. Scherer, T. S. Bischof, M. Wu, N. Geva, M. Welborn, T. V. Voorhis, V. Bulović, M. G. Bawendi, and M. A. Baldo. Energy harvesting of non-emissive triplet excitons in tetracene by emissive PbS nanocrystals. *Nature Materials* **2014**, *13*(*11*), 1039–1043.

[108] C. Mongin, S. Garakyaraghi, N. Razgoniaeva, M. Zamkov, and F. N. Castellano. Direct observation of triplet energy transfer from semiconductor nanocrystals. *Science* **2016**, *351*(*6271*), 369–372.

[109] L. Hou, A. Olesund, S. Thurakkal, X. Zhang, and B. Albinsson. Efficient Visible-to-UV Photon Upconversion Systems Based on CdS Nanocrystals Modified with Triplet Energy Mediators. *Advanced Functional Materials* **2021**, *31*(*47*), 2106198.

[110] W. W. Yu and X. Peng. Formation of High-Quality CdS and Other II–VI Semiconductor Nanocrystals in Noncoordinating Solvents: Tunable Reactivity of Monomers. *Angewandte Chemie International Edition* **2002**, *41*(*13*), 2368–2371.

[111] Z. Li, Y. Ji, R. Xie, S. Y. Grisham, and X. Peng. Correlation of CdS Nanocrystal Formation with Elemental Sulfur Activation and Its Implication in Synthetic Development. *Journal of the American Chemical Society* **2011**, *133*(*43*), 17248–17256.

[112] M. Irie, K. Sakemura, M. Okinaka, and K. Uchida. Photochromism of Dithienylethenes with Electron-Donating Substituents. *The Journal of Organic Chemistry* **1995**, *60*(*25*), 8305–8309.

[113] K. Sandros. Transfer of Triplet State Energy in Fluid Solutions. III. Reversible Energy Transfer. *Acta Chemica Scandinavica* **1964**, *18*, 2355–2374.

[114] W. Larsson, M. Morimoto, M. Irie, J. Andréasson, and B. Albinsson. Diarylethene isomerization by using triplet–triplet annihilation photon upconversion. *Chemistry – A European Journal* **2023**, *29*(*13*), e202203651.

[115] R. R. Islangulov and F. N. Castellano. Photochemical Upconversion: Anthracene Dimerization Sensitized to Visible Light by a Ru^{II} Chromophore. *Angewandte Chemie International Edition* **2006**, *45*(*36*), 5957–5959.

[116] S. H. Askes, A. Bahreman, and S. Bonnet. Activation of a photodissociative ruthenium complex by triplet-triplet annihilation upconversion in liposomes. *Angewandte Chemie International Edition* **2014**, *53*(*4*), 1029–1033.

[117] M. Majek, U. Faltermeier, B. Dick, R. Pérez-Ruiz, and A. Jacobi von Wangelin. Application of Visible-to-UV Photon Upconversion to Photoredox Catalysis: The Activation of Aryl Bromides. *Chemistry - A European Journal* **2015**, *21*(*44*), 15496–15501.

[118] B. D. Ravetz, A. B. Pun, E. M. Churchill, D. N. Congreve, T. Rovis, and L. M. Campos. Photoredox catalysis using infrared light via triplet fusion upconversion. *Nature* **2019**, *565*(*7739*), 343–346.

[119] B. Pfund, D. M. Steffen, M. R. Schreier, M.-S. Bertrams, C. Ye, K. Börjesson, O. S. Wenger, and C. Kerzig. UV Light Generation and Challenging Photoreactions Enabled by Upconversion in Water. *Journal of the American Chemical Society* **2020**, *142*(*23*), 10468–10476.

[120] L. Huang, L. Zeng, Y. Chen, N. Yu, L. Wang, K. Huang, Y. Zhao, and G. Han. Long wavelength single photon like driven photolysis via triplet triplet annihilation. *Nature Communications* **2021**, *12*(*1*), 122.

[121] A. Tokunaga, L. M. Uriarte, K. Mutoh, E. Fron, J. Hofkens, M. Sliwa, and J. Abe. Photochromic Reaction by Red Light via Triplet Fusion Upconversion. *Journal of the American Chemical Society* **2019**, *141*(*44*), 17744–17753.

[122] J. B. Bilger, C. Kerzig, C. B. Larsen, and O. S. Wenger. A Photorobust Mo(0) Complex Mimicking $[Os(2,2\text{-bipyridine})_3]^{2+}$ and Its Application in Red-to-Blue Upconversion. *Journal of the American Chemical Society* **2021**, *143*(*3*), 1651–1663.

[123] R. Nishimura, E. Fujisawa, I. Ban, R. Iwai, S. Takasu, M. Morimoto, and M. Irie. Turn-on mode fluorescent diarylethene containing neopentyl substituents that undergoes all-visible-light switching. *Chemical Communications* **2022**, *58*(*30*), 4715–4718.

[124] K. Uno, H. Niikura, M. Morimoto, Y. Ishibashi, H. Miyasaka, and M. Irie. In situ preparation of highly fluorescent dyes upon photoirradiation. *Journal of the American Chemical Society* **2011**, *133*(*34*), 13558–13564.

[125] Q. Liu, T. Yang, W. Feng, and F. Li. Blue-emissive upconversion nanoparticles for low-power-excited bioimaging in vivo. *Journal of the American Chemical Society* **2012**, *134*(*11*), 5390–5397.

[126] L. Huang, T. Le, K. Huang, and G. Han. Enzymatic enhancing of triplet–triplet annihilation upconversion by breaking oxygen quenching for background-free biological sensing. *Nature Communications* **2021**, *12*(*1*), 1898.

[127] S. N. Sanders, T. H. Schloemer, M. K. Gangishetty, D. Anderson, M. Seitz, A. O. Gallegos, R. C. Stokes, and D. N. Congreve. Triplet fusion upconversion nanocapsules for volumetric 3D printing. *Nature* **2022**, *604*(*7906*), 474–478.

[128] J.-H. Kim and J.-H. Kim. Encapsulated triplet–triplet annihilation-based upconversion in the aqueous phase for sub-band-gap semiconductor photocatalysis. *Journal of the American Chemical Society* **2012**, *134*(*42*), 17478–17481.

[129] J. D. Rule, N. R. Sottos, and S. R. White. Effect of microcapsule size on

the performance of self-healing polymers. *Polymer* **2007**, *48*(*12*), 3520–3529.

[130] B. Städler, R. Chandrawati, A. D. Price, S.-F. Chong, K. Breheney, A. Postma, L. A. Connal, A. N. Zelikin, and F. Caruso. A microreactor with thousands of subcompartments: Enzyme-loaded liposomes within polymer capsules. *Angewandte Chemie International Edition* **2009**, *48*(*24*), 4359–4362.

[131] Y. Su, B. Zhang, R. Sun, W. Liu, Q. Zhu, X. Zhang, R. Wang, and C. Chen. PLGA-based biodegradable microspheres in drug delivery: recent advances in research and application. *Drug Delivery* **2021**, *28*(*1*), 1397–1418.

[132] D. Dzebo, K. Moth-Poulsen, and B. Albinsson. Robust triplet-triplet annihilation photon upconversion by efficient oxygen scavenging. *Photochemical and Photobiological Sciences* **2017**, *16*(*8*), 1327–1334.

[133] T. E. Karis and H. S. Nagaraj. Evaporation and flow properties of several hydrocarbon oils. *Tribology Transactions* **2000**, *43*(*4*), 758–766.